Islamic University of Gaza
Research & Graduate Affairs
Faculty of Science
Department of Physics

NOVEL SLAB WAVEGUIDE OPTICAL SENSORS

تراكيب جديدة لمجسات الموجهات الضوئية

By

Sameh Saleem Mahdi

Supervisor

Dr. Sofyan A. Taya
Associate Professor in Physics

A Thesis Submitted in Partial Fulfillment of the Requirements
for the Degree of Master in Physics.

1435-2014

Dedication

To my affectionate parents who always had faith in me and supported me.

To my compassionate brother and sisters who also had faith in me and encouraged me constantly.

To my tender soulful wife for her endless support .

To my children for their patience.

Acknowledgment

In the name of Allah to whom I am overwhelmed with gratitude for continuous help and guidance throughout the path of knowledge.

To the Islamic university in general and the Physics department in special for the opportunity they gave me. To all ones who helped, supported and encouraged me all the way till this point.

I appreciate deeply Prof. Mohammed Shabat who inspired me in this subject and who taught me how to look for information.

It has been a great pleasure to work under supervision of Dr. Sofyan Taya who helped, assisted and encouraged me in all stages of my work. I am very grateful for his invaluable help, guidance and his enthusiasm.

Abstract

An optical slab waveguide sensor is proposed. The structure of the proposed sensor consists of three-layer dielectric slab waveguide with conducting layers at the interfaces. The dispersion relation, sensitivity, and power flow are derived for transverse electric (TE) and transverse magnetic (TM) polarizations. Positive and negative surface conductivities are considered at the substrate/film and film/cladding interfaces. The enhancement of the sensing sensitivity of the effective refractive index to any variation in the index of an analyte is shown for a wide range of the surface conductivity. A sensitivity improvement of more than 150% is found compared to the conventional slab waveguide sensor.

Compared to other waveguide sensors, the proposed sensor differs in that the sensitivity can be controlled or adjusted without changing the waveguide structure. It is resembles using the focusing in the microscope to get clearer image of the specimen using the coarse and fine focus adjustment. Adjusting the sensor's sensitivity can be done by changing the surface conductivity using a transverse voltage.

ملخص البحث

مقترح لمجس موجه ضوئي جديد، يتكون المجس الجديد من موجه مسطح مكون من ثلاث طبقات من مواد عازلة بوجود موصلية سطحية على السطوح البينية، وقد تم اشتقاق معادلات التشتت والحساسية وتدفق الطاقة لكل من حالتي الاستقطاب : المجال الكهربي المستعرض والمجال المغناطيسي المستعرض. تمت الدراسة لكل من حالتي الموصلية السطحية الموجبة والسالبة على السطوح البينية للفيلم/ الركيزة والفيلم/العينة، وقد تبين وجود تحسين في حساسية المجس بإضافة الموصلية السطحية للمجس.

يمتاز المجس المقترح عن مجسات الموجهات الضوئية الأخرى بإمكانية التحكم بالحساسية بدون تغيير تركيب المجس، وذلك بتغيير الموصلية السطحية باستخدام فرق جهد عرضي، ويتشابه ذلك مع استخدام المجهر في الحصول على صورة أوضح للعينة باستخدام ضابطي التركيز:الكبير والصغير.

Table of Contents

List of Figures

Chapter One

Chapter Two

Chapter Three

Chapter one

Review of Electromagnetic and Waveguide Theories

Introduction

The study of slab waveguide sensors requires a good understanding of electromagnetic field theory and basics of slab waveguides. This chapter consists of two parts, part I gives a review of electromagnetism and part II discusses the waveguide theory.

In part I Maxwell's equations and the constitutive relationships are presented. The wave equation is then derived and the boundary conditions for the fields at an interface between two media are studied.

In part II the solution of the wave equation derived in part I is used, along with the boundary conditions, to derive the dispersion relations for both transverse electric (TE) and transverse magnetic (TM) modes.

Part I

1.1 Electromagnetic Theory

The propagation of electromagnetic waves is fully described by Maxwell's equations (ME's) and the constitutive relations sometimes called material equations [1]. ME's describe the relation between the electric and magnetic fields constituting the electromagnetic waves, while the constitutive equations describe the interaction between those fields and media.

1.1.1 Maxwell's Equations

It was thought that electricity and magnetism were two separate forces. Until the Scottish physicist and mathematician James Clerk Maxwell published a four-part paper, "On Physical Lines of Force" between 1861 and 1862. In his paper, he formulated a set of equations that connected previously unrelated

observations, experiments, and equations of electricity, magnetism, and optics into a consistent theory. Maxwell's equations are four equations that gather the work of Gauss, Faraday and Ampere in one theory, the theory of classical electromagnetism, after correcting Ampere's law by adding the displacement current.

Maxwell's equations can be written in many forms. There are the microscopic and macroscopic forms. There are also the differential and integral forms. The differential form of Maxwell's equations is given by

$$\nabla \times \vec{E} = -\frac{\partial \vec{B}}{\partial t}, \tag{1.1}$$

$$\nabla \times \vec{H} = \frac{\partial \vec{D}}{\partial t} + \vec{J}, \tag{1.2}$$

$$\nabla . \vec{D} = \rho, \tag{1.3}$$

$$\nabla . \vec{B} = 0, \tag{1.4}$$

where $\vec{E}$ and $\vec{H}$ are the electric and magnetic fields, respectively, $\vec{D}$ and $\vec{B}$ are the electric and magnetic flux densities, respectively, and ρ and $\vec{J}$ are the electric charge and the current densities, respectively.

1.1.2 Constitutive Relations

The fields and flux densities in Eqs. (1.1)-(1.4) are related to each other by the constitutive relations.

For a linear, isotropic, homogeneous medium

$$\vec{D} = \varepsilon \vec{E}, \tag{1.5}$$

$$\vec{B} = \mu \vec{H} \,, \tag{1.6}$$

$$\vec{J} = \sigma \vec{E} \,, \tag{1.7}$$

where ε and μ are the electric permittivity and the magnetic permeability of the medium , respectively, and σ is the surface conductivity.
The permittivity and permeability of a medium can be written as

$$\varepsilon = \varepsilon_0 \, \varepsilon_r \,, \tag{1.8}$$

$$\mu = \mu_0 \, \mu_r \,, \tag{1.9}$$

where ε_0 is the permittivity of vacuum and equals $8.854 \times 10^{-12} F/m$ and ε_r is the relative permittivity of the medium. μ_0 is the permeability of vacuum and equals to $4\pi \times 10^{-7} H/m$ and μ_r is the relative permeability of the medium.

For anisotropic material the permittivity and permeability take the forms of a second rank tensor.

$$\bar{\varepsilon} = \begin{pmatrix} \varepsilon_{xx} & \varepsilon_{xy} & \varepsilon_{xz} \\ \varepsilon_{yx} & \varepsilon_{yx} & \varepsilon_{yz} \\ \varepsilon_{zx} & \varepsilon_{zy} & \varepsilon_{zz} \end{pmatrix} \quad \text{and} \qquad \bar{\mu} = \begin{pmatrix} \mu_{xx} & \mu_{xy} & \mu_{xz} \\ \mu_{yx} & \mu_{yy} & \mu_{yz} \\ \mu_{zx} & \mu_{zy} & \mu_{zz} \end{pmatrix}. \tag{1.10}$$

This is the most general form of both the permittivity and permeability of an anisotropic material. This means that the x, y and z-components of the electric flux and magnetic flux densities, $\vec{D}$ and $\vec{B}$ respectively, depend on the x, y and z-components of the electric and magnetic fields, $\vec{E}$ and $\vec{H}$, respectively.

1.1.3 Wave Equation

Taking the curl of Eq. (1.1) to derive the wave equation

$$\nabla \times \nabla \times \vec{E} = -\mu \frac{\partial}{\partial t}\left(\nabla \times \vec{H}\right). \tag{1.11}$$

Substituting Eq. (1.2) into (1.11), taking into account non-conducting media i.e. $\vec{J}$=0,

$$\nabla \times \nabla \times \vec{E} = -\mu \frac{\partial^2 \vec{D}}{\partial t^2} = -\mu\varepsilon \frac{\partial^2 \vec{E}}{\partial t^2}. \tag{1.12}$$

Using the vector identity

$$\nabla \times \nabla \times \vec{E} = \nabla(\nabla.\vec{E}) - \nabla^2 \vec{E}. \tag{1.13}$$

Substituting Eq.(1.13) into (1.12)

$$\nabla^2 \vec{E} - \mu\varepsilon \frac{\partial^2 \vec{E}}{\partial t^2} = \nabla\left(\nabla.\vec{E}\right). \tag{1.14}$$

For a source free isotropic medium $\nabla.\vec{E}$=0 from Eq. (1.3), so that Eq. (1.14) becomes

$$\nabla^2 \vec{E} - \mu\varepsilon \frac{\partial^2 \vec{E}}{\partial t^2} = 0. \tag{1.15}$$

Similarly, starting with Eq. (1.2) and following the above procedure we get

$$\nabla^2 \vec{H} - \mu\varepsilon \frac{\partial^2 \vec{H}}{\partial t^2} = 0. \tag{1.16}$$

Equations (1.15) and (1.16) are three dimensional equations where the laplacian operator ∇^2 is given in rectangular coordinates by

$$\nabla^2 = \frac{\partial^2}{\partial x^2} + \frac{\partial^2}{\partial y^2} + \frac{\partial^2}{\partial z^2} . \qquad (1.17)$$

Equations (1.15) and (1.16) are called Helmholtz equations which have a sinusoidal solution if the coefficient of the second term is positive and an exponentially increasing or decreasing solution if it is negative.
The ideal notation for the electromagnetic wave which represents the solution of the wave equation, is the phasor notation, i.e.

$$\vec{\psi}\left(\vec{r}, t\right) = \psi_0 e^{-i(\vec{k}.\vec{r} - \omega t)} , \qquad (1.18)$$

where $\vec{\psi}$ is either $\vec{E}$ or $\vec{H}$, ψ_0 is the amplitude of the wave, $\vec{k}$ is the wave vector and ω is the angular frequency.

Applying the phasor notation to Maxwell's equations, we get

$$\nabla \times \vec{E} = i\omega\mu\vec{H} , \qquad (1.19)$$

$$\nabla \times \vec{H} = -i\omega\varepsilon\vec{E} . \qquad (1.20)$$

Helmholtz equation for either $\vec{E}$ or $\vec{H}$ becomes

$$\nabla^2\vec{\psi} - \mu\varepsilon\omega^2\vec{\psi} = \nabla^2\vec{\psi} - \frac{\omega^2}{v^2}\vec{\psi} = 0 , \qquad (1.21)$$

where v is the speed of light in the medium.

1.1.4 Boundary Conditions

During the propagation of electromagnetic wave from one medium to another, it obeys some conditions at the interface between the two media. These are the boundary conditions [1] which can be summarized as

1- The normal component of the magnetic flux is continuous across the surface of discontinuity, i.e.

$$\hat{n}_{12}.\left(\vec{B}_2 - \vec{B}_1\right) = 0\,, \tag{1.22}$$

where $\hat{n}_{12}$ is a unit vector normal to the interface.

2- In the presence of a surface charge of density ρ, the normal component of the electric displacement is discontinuous by ρ, i.e.

$$\hat{n}_{12}.\left(\vec{D}_2 - \vec{D}_1\right) = \rho\,. \tag{1.23}$$

From the above equation it is clear that in the absence of the surface charge the electric displacement is continuous.

3- The tangential component of the electric field is continuous across the surface, i.e.

$$\hat{n}_{12} \times \left(\vec{E}_2 - \vec{E}_1\right) = 0\,. \tag{1.24}$$

4- In the presence of a surface current of density $\vec{J}$, the tangential component of the magnetic field is discontinuous across the surface by $\vec{J}$, i.e.

$$\hat{n}_{12} \times \left(\vec{H}_2 - \vec{H}_1\right) = \vec{\mathrm{J}}\,. \tag{1.25}$$

The importance of the boundary conditions gets clear when dealing with electromagnetic waves striking an interface between two different media.

1.1.5 Medium and Wave Parameters

All media are characterized by some parameters which give them their physical properties. In the electromagnetic theory, the most important parameters are the permittivity and permeability. In optics, media are basically characterized by the refractive index, which is defined as the ratio of the speed of light in vacuum to its speed in the medium.

$$n = \frac{c}{\upsilon}. \tag{1.26}$$

Since $c = \frac{1}{\sqrt{\varepsilon_0 \mu_0}}$ and from Eqs. (1.8), (1.9) and (1.21), the speed of light in any medium is given by $v = \frac{c}{\sqrt{\varepsilon_r \mu_r}}$. One may conclude that the refractive index is given by

$$n = \sqrt{\varepsilon_r \mu_r}. \tag{1.27}$$

When light propagates through a medium and being absorbed, the medium is said to be lossy. There is another parameter that should mentioned when dealing with lossy materials. This parameter is the extinction coefficient which is denoted by κ [2]. The intensity of the wave will decrease exponentially when propagating in such media. In this case the complex refractive index $(\tilde{n})$ is introduced which is given by

$$\tilde{n} = n + i\kappa, \tag{1.28}$$

where n is given by Eqs. (1.26) and (1.27), while κ is the extinction coefficient.

As a result, both the permittivity and permeability are also complex, and given by $\tilde{\varepsilon} = \varepsilon_r + i\varepsilon_i$ and $\tilde{\mu} = \mu_r + i\mu_i$.

It is worth to mention that the refractive index n and the extinction coefficient κ are not independent parameters, they are connected to each other by Kramers-Kronig relations [2] which are given by

$$n(\omega) = 1 + \frac{1}{\pi} P \int_{-\infty}^{+\infty} \frac{\kappa(\omega')}{\omega' - \omega} d\omega', \tag{1.29}$$

$$\kappa(\omega) = -\frac{1}{\pi} P \int_{-\infty}^{+\infty} \frac{n(\omega')}{\omega' - \omega} d\omega'. \tag{1.30}$$

The P indicates that the integral is taken over the principal part.

It is clear that the parameters of a medium are closely related to the wave parameters. The main wave parameters are the frequency ν and wavelength λ, from which we can get the angular frequency ω and the wave number k, where $\omega = 2\pi\nu$ and $k = 2\pi/\lambda$.

The wave number in free space is given by

$$k_0 = \frac{2\pi}{\lambda_0}, \tag{1.31}$$

where the $_0$ denotes the parameter in free space. Consequently, we can get the wave parameters in a medium if the wave free space parameters and its refractive index are known

$$\lambda = \frac{\lambda_0}{n} \text{ and } k = nk_0. \tag{1.32}$$

As a result if the medium has a complex refractive index the wave vector will also be complex.

1.1.6 Reflection and Refraction

In homogeneous and isotropic media electromagnetic waves propagate in straight lines. But during its propagations in a medium, if the wave impinges an interface with another medium, it might be completely reflected back in the same medium, completely transmitted into the second medium or partially reflected and partially transmitted. The situation depends on the parameters of both media, specifically the refractive indices, and the angle of incidence, i.e. the angle which the ray makes with the normal to the interface.

The first case is discussed in the next section while the second case is discussed at the end of this section. The last case can be explained as follows. Consider two adjacent dielectric media with the interface separating them in the x-y plane. An electromagnetic wave with the electric field perpendicular to the plane of incidence, TE polarized wave, is incident from medium I with refractive index n_i to medium II with refractive index n_t as shown in Fig. 1.1.

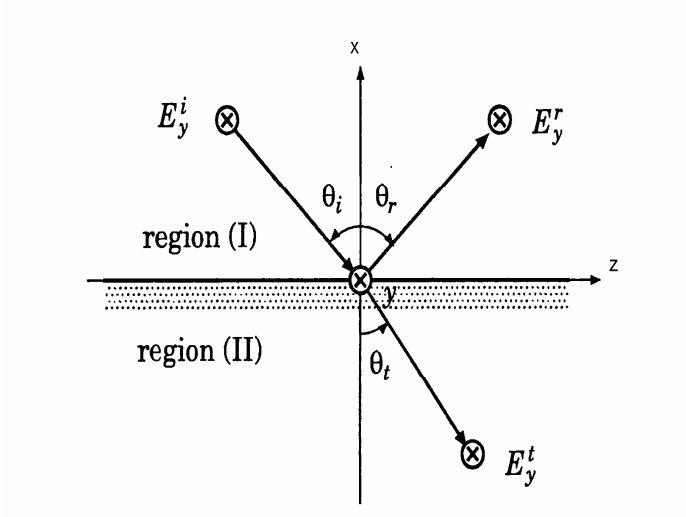

Fig. 1.1 An electromagnetic wave incident at a plane interface.

In this case part of the wave is reflected back in the first medium and the other part is transmitted into the second medium. Reflection obeys the following laws:

1. The incident ray, the reflected ray and the normal to the reflection surface at the point of incidence lie in the same plane.
2. The angle of reflection (θ_r) equals the angle of incidence.
3. The reflected and incident rays are on the opposite sides of the normal.

While the refraction laws are:

1. The incident ray, the refracted ray and the normal to the reflection surface at the point of incidence lie in the same plane.
2. The angle of the refracted ray (θ_t) is governed by Snell's law,

$$n_i \sin\theta_i = n_t \sin\theta_t . \tag{1.33}$$

The refraction occurs because the phase velocity of the wave changes, which causes the change in direction. As a result, the wavelength is altered while the frequency remains constant.

The reflection (r) and transmission (t) coefficients are given by Fresnel equations

$$r_{TE} = \frac{n_i \cos\theta_i - n_t \cos\theta_t}{n_i \cos\theta_i + n_t \cos\theta_t}, \tag{1.34}$$

$$t_{TE} = \frac{2n_i \cos\theta_i}{n_i \cos\theta_i + n_t \cos\theta_t}, \tag{1.35}$$

$$r_{TM} = \frac{n_t \cos\theta_i - n_i \cos\theta t}{n_i \cos\theta_t + n_t \cos\theta_i}, \tag{1.36}$$

$$t_{TM} = \frac{2n_i \cos\theta_i}{n_i \cos\theta_t + n_t \cos\theta_i}, \tag{1.37}$$

where TE and TM denote transverse electric and transverse magnetic polarizations respectively.

There is a special angle of incidence at which the wave is totally transmitted i.e. there's no reflection. This angle is called Brewster's angle. For an interface between two right-handed materials of positive refractive indices, Brewster angle only exists for TM polarized waves. While if one of the media is a left-handed material with negative index of refraction zero reflection can be found for both polarizations [3]. Generally, Brewster angle is given by

$$\cos^2\theta_{B_{TE}} = \frac{\varepsilon_t/\varepsilon_i - \mu_i/\mu_t}{\mu_t/\mu_i - \mu_i/\mu_t}, \tag{1.38}$$

$$\cos^2\theta_{B_{TM}} = \frac{\mu_t/\mu_i - \varepsilon_i/\varepsilon_t}{\varepsilon_t/\varepsilon_i - \varepsilon_i/\varepsilon_t}. \tag{1.39}$$

1.1.7 Total Internal Reflection (TIR) and Evanescent Fields

Under certain conditions a wave striking an interface between two different media is being totally reflected back into the first medium and θ_t becomes 90°, i.e. there is no transmission. This phenomenon is called total internal reflection, and it takes place when the second medium is less denser than the first medium, i.e. $n_1 > n_2$, and the angle of incidence is greater than a particular angle called the critical angle (θ_c), as shown in Fig.1.2. The critical angle is given by

$$\theta_c = \sin^{-1}\left(\frac{n_2}{n_1}\right). \tag{1.40}$$

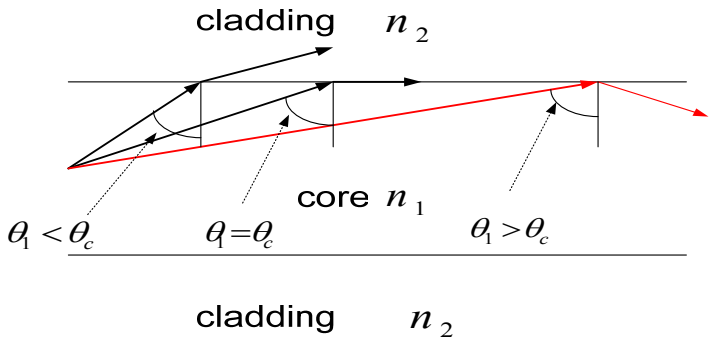

Fig. 1.2. Refraction of light at different angles including TIR.

TIR is a very important phenomena as it is the basic principle for operation of waveguides of all kinds.

An important result of TIR is the propagation of an evanescent wave across the interface. Essentially, even though the entire incident wave is reflected back into the first medium, there is some penetration into the second medium at the boundary, as shown below

For $\theta_i > \theta_c$, from Snell's law it can be shown that

$$\cos\theta_t = i\sqrt{\frac{n_1^2}{n_2^2}\sin^2\theta_i - 1}\,. \tag{1.41}$$

The transmitted electric field is given by:

$$\vec{E}_t = E_{t0}\exp\left(-ik_2(z\cos\theta_t - y\sin\theta_t\right). \tag{1.42}$$

So that,

$$\vec{E}_t = E_{t0}\exp\left(ik_2 y\frac{n_1}{n_2}\sin\theta_i\right)\exp\left(-k_2 z\sqrt{\frac{n_1^2}{n_2^2}\sin^2\theta_i - 1}\right). \tag{1.43}$$

As seen from Fig.1.3. and Eq. (1.43), the refracted wave propagates only parallel to the surface and is attenuated exponentially in the second medium.

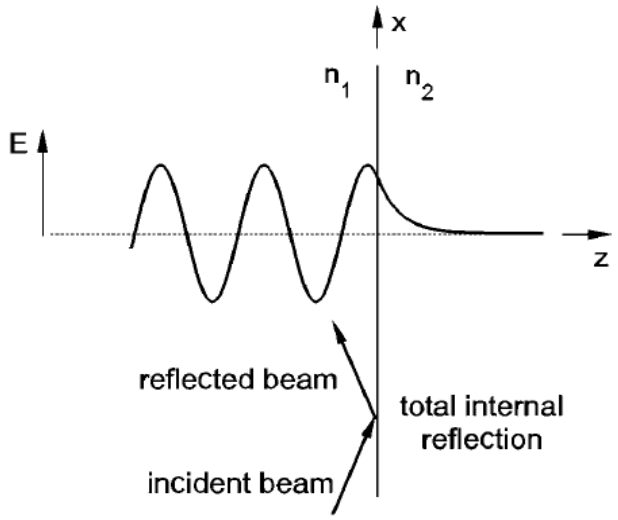

Fig. 1.3. Evanescent wave in medium 2 after TIR.

Another aspect of TIR, is that the evanescent wave appears to travel along the boundary between the two materials, leading to the Goos-Hänchen shift. The wave makes a lateral shift along the interface and does not reflect back at the same point it strikes the interface as shown in Fig. 1.4. The magnitude of the shift depends on the polarization.

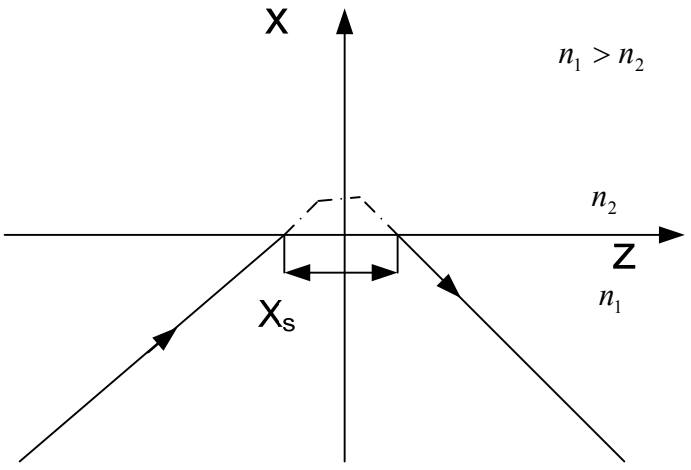

Fig. 1.4 Goos-Hänchen shift effect.

The explanation of this shift is that the incident light first penetrates the low-index medium as an evanescent wave before being totally reflected back into the high-index medium [4].

Part II

1.2 Waveguide Theory

In this part, principles developed in part I are used to discuss the theory of waveguides. In particular, the planar dielectric step index waveguide will be studied. Dispersion relations will be derived for both TE and TM modes.

1.2.1 Introduction

A waveguide is a dispersive structure that confines and directs a wave. In other words, it conveys a wave between its ends. An optical waveguide is used to guide waves in the optical spectrum.

The first waveguide was proposed by J.J. Thomson in 1893, and was experimentally verified by O.J. Lodge in 1894.

Optical waveguides utilize the TIR phenomena to confine and convey light.

There are many aspects to classify optical waveguides, they can be classified according to:

1- Geometrical shape: planar, strip or fiber waveguides.
2- Mode structure: single-mode or multimode.
3- Refractive index distribution: step-index or graded-index.
4- Material: glass, polymer or semiconductor.

Light was first guided by Daniel Colladon, a 38-year-old professor at the University of Geneva in 1841 [5,6]. He illuminated a barrel full of water from one side, with holes in the other side of the barrel. Light was confined in the water flowing from the holes instead of propagating in straight lines.

1.2.2 Waveguide Structure

Fig.1.5. shows the structure of the basic dielectric step index waveguide, which consists of three adjacent plane layers: a core (film), cladding (cover) and substrate. The film is sandwiched between the cover and substrate and it has the highest refractive index n_f. The film thickness is thin and comparable to the operating wavelength. While the substrate and cover are relatively thick and have refractive indices n_s and n_c respectively such that $n_f > n_s > n_c$. The thickness of both cover and substrate is much larger than the wavelength so that they are considered as semi-infinite media.

The change in the refractive index of the three layers is sharp.

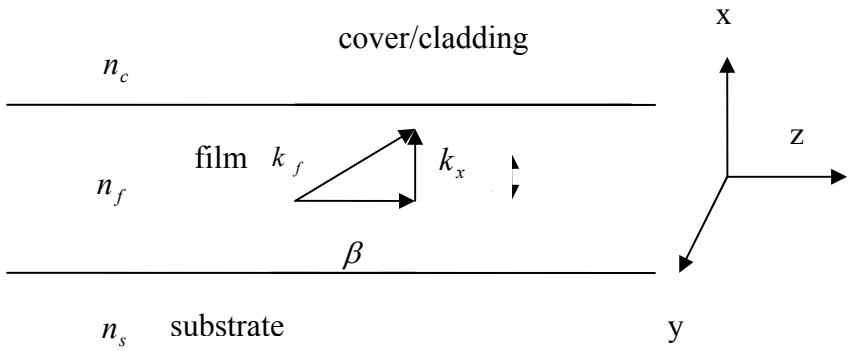

Fig. 1.5. Basic structure of the dielectric planar waveguide.

As mentioned above, light is confined in the core of a planar waveguide by TIR at both film/cover and film/substrate interfaces as shown in Fig. 1.6. This occurs when the refractive index of the film is greater than those of cover and substrate. Consequently, light will be reflected back and forth between the two interfaces till it is transmitted.

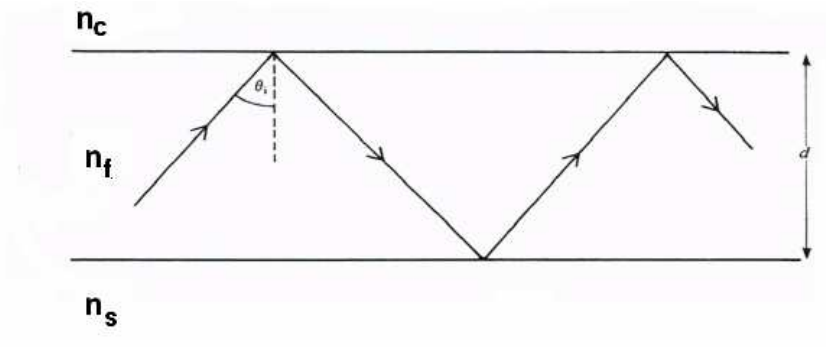

Fig. 1.6. Light confinement in a planar waveguide by TIR.

1.2.3 Formulation of Waveguide Equations

The analysis of planar waveguide requires solving Helmholtz equation in the three layers and applying the boundary conditions at each interface.

Consider again the waveguide shown in Fig. 1.5. The wave is supposed to propagate in the z-direction. The waveguide is assumed to be infinitely extended in the y-direction, so that there's symmetry in the field distribution in this direction and imposes that $\frac{\partial}{\partial y} = 0$.

Expanding Eq. (1.1) in three dimensions using the phasor notation for the harmonic waves, we get

$$\begin{vmatrix} \hat{i} & \hat{j} & \hat{k} \\ \partial/\partial x & \partial/\partial y & \partial/\partial z \\ E_x & E_y & E_z \end{vmatrix} = -i\mu\omega(H_x\hat{i} + H_y\hat{j} + H_z\hat{k}). \qquad (1.44)$$

Let β be the longitudinal propagation constant, so $\frac{\partial}{\partial z} = -i\beta$, and using the fact $\frac{\partial}{\partial y} = 0$ we get

$$\beta E_y = -\omega\mu H_x, \qquad (1.45)$$

$$i\beta E_x + \frac{\partial E_z}{\partial x} = i\omega\mu H_y, \tag{1.46}$$

$$\frac{\partial E_y}{\partial x} = -i\omega\mu H_z. \tag{1.47}$$

In a similar manner, expanding Eq.(1.2) gives

$$\begin{vmatrix} \hat{i} & \hat{j} & \hat{k} \\ \partial/\partial x & \partial/\partial y & \partial/\partial z \\ H_x & H_y & H_z \end{vmatrix} = i\varepsilon\omega(E_x\hat{i} + E_y\hat{j} + E_z\hat{k}). \tag{1.48}$$

We get

$$\beta H_y = \omega\varepsilon E_x, \tag{1.49}$$

$$i\beta H_x + \frac{\partial H_z}{\partial x} = -i\omega\varepsilon E_y, \tag{1.50}$$

$$\frac{\partial H_y}{\partial x} = i\omega\varepsilon E_z. \tag{1.51}$$

1.2.3.1 Transverse Electric (TE) Modes

TE polarization is in which the electric field vector of the incident wave is parallel to the interface between the layers. In our model there's a non-zero y-component of the electric field, while we have non-zero x and z-components of the magnetic field. In other words, $E_x = E_z = H_y = 0$.

From Eqs. (1.45), (1.47) and (1.50) we get

$$\frac{\partial^2 E_y}{\partial x^2} + k_0^2(n^2 - N^2)E_y = 0, \tag{1.52}$$

where $N = \frac{\beta}{k_0}$ is the effective refractive index of the waveguide, and k_0 is the wave number in vacuum. The solutions of Eq. (1.52) in the three layers is given by

$$E_y(x) = \begin{cases} Ae^{-\alpha_c(x-d)}, x > d \\ B_1 \cos(\alpha_f x) + B_2 \sin(\alpha_f x), 0 < x < d \\ Ce^{\alpha_s x}, x < 0 \end{cases}, \quad (1.53)$$

where A, B_1, B_2 and C are constants to be determined, d is the film thickness and

$$\alpha_c = k_0 \sqrt{N^2 - n_c^2}, \quad (1.54)$$

$$\alpha_f = k_0 \sqrt{n_f^2 - N^2}, \quad (1.55)$$

and

$$\alpha_s = k_0 \sqrt{N^2 - n_s^2}. \quad (1.56)$$

Applying the boundary conditions for source free media we get the transverse resonance condition, also called the dispersion relation, for the allowed modes for TE polarization

$$\alpha_f d = \tan^{-1} \gamma_c + \tan^{-1} \gamma_s + m\pi, \quad (1.57)$$

where m=0, 1, 2,… is the mode order and

$$\gamma_c = \frac{\alpha_c}{\alpha_f} \text{ and } \gamma_s = \frac{\alpha_s}{\alpha_f}. \quad (1.58)$$

As can be seen from Eq. (1.57) there are discrete values of the longitudinal wave vector β that satisfy the transverse resonance condition. These allowed solutions are called modes.

1.2.3.2 Transverse Magnetic (TM) Modes

TM polarization is in which the magnetic field vector of the incident wave is parallel to the interface between the layers. So there's a non-zero y-component of the magnetic field, while we have non-zero x and z-components of the electric field. In other words, $H_x = H_z = E_y = 0$.

From Eqs. (1.46), (1.49) and (1.51) we get

$$\frac{\partial^2 H_y}{\partial x^2} + k_0^2 (n^2 - N^2) H_y = 0 . \tag{1.59}$$

Solving the above equation in the three layers and applying the boundary conditions we get the transverse resonance condition for TM polarization as follows:

$$\alpha_f d = \tan^{-1} \delta_c + \tan^{-1} \delta_s + m\pi , \tag{1.60}$$

where,

$$\delta_c = \frac{\alpha_c \varepsilon_f}{\alpha_f \varepsilon_c} \text{ and } \delta_s = \frac{\alpha_s \varepsilon_f}{\alpha_f \varepsilon_s} \quad . \tag{1.61}$$

1.2.4 Power Considerations

Electromagnetic waves carry energy. At any point in space, the flow of energy can be described by a power density vector $\vec{P}$, which specifies both the power

density and the direction of flow. The vector $\vec{P}$ is called Poynting vector and is given by

$$\vec{P} = \vec{E} \times \vec{H} \,. \tag{1.62}$$

Since $\vec{P}$ represents a physical quantity it should be real, so only real parts of the three vectors in Eq. (1.62) should be considered. Moreover, it is more convenient to deal with the average of the Poynting vector for time harmonic fields as in Eq. (1.18).

$$\vec{P}_{av} = \frac{1}{T}\int_0^T dt\left[\mathrm{Re}\,\vec{E} \times \mathrm{Re}\,\vec{H}\right]. \tag{1.63}$$

Using phasor notation and Maxwell's equations, Eq. (1.63) yields [3]

$$\vec{P}_{av} = \frac{1}{2\omega}\mathrm{Re}[\frac{\vec{k}}{\mu}\left|E\right|^2] = \frac{1}{2\omega}\mathrm{Re}[\frac{\vec{k}}{\varepsilon}\left|H\right|^2]. \tag{1.64}$$

Eq. (1.64) is valid in a homogeneous medium. For an inhomogeneous medium such as a waveguide as in Fig. 1.5. the power is distributed in the three layers. The average Poynting vector is given by

$$\vec{P}_{total} = \frac{1}{2\omega}\int_{-\infty}^{\infty}\mathrm{Re}[\frac{\beta}{\mu_i(x)}\left|E_y(x)\right|^2]dx\,, \tag{1.65}$$

For TE polarization.
Consequently the power confined in the three layers is given by [7]

$$P_{c_{TE}} = \left(\frac{\beta}{2\omega\mu}\right)\frac{A^2}{2\alpha_c}, \tag{1.66}$$

$$P_{f_{TE}} = \left(\frac{\beta}{2\omega\mu}\right)\frac{A^2}{2}\left(\frac{\alpha_f^2+\alpha_c^2}{\alpha_f^2}\right)\left[d+\frac{\alpha_s}{\alpha_f^2+\alpha_s^2}+\frac{\alpha_c}{\alpha_f^2+\alpha_c^2}\right], \tag{1.67}$$

$$P_{s_{TE}} = \left(\frac{\beta}{2\omega\mu}\right)\frac{A^2}{2\alpha_s}\left(\frac{\alpha_f^2+\alpha_c^2}{\alpha_f^2+\alpha_s^2}\right), \tag{1.68}$$

where

$$A^2 = \frac{P_{total}}{\left(\frac{\beta}{2\omega\mu}\right)\left(\frac{\alpha_f^2+\alpha_c^2}{2\alpha_f^2}\right)\left(d+\frac{1}{\alpha_s}+\frac{1}{\alpha_c}\right)}, \tag{1.69}$$

$$P_{total} = P_{c_{TE}} + P_{f_{TE}} + P_{s_{TE}}, \tag{1.70}$$

and α_c, α_f and α_s are given by Eqs. (1.54-1.56).

Similar expressions can be obtained for TM polarization using the relation

$$\vec{P}_{total} = \frac{1}{2\omega}\int_{-\infty}^{\infty}\mathrm{Re}\left[\frac{\beta}{\varepsilon_i(x)}\left|H_y(x)\right|^2\right]dx. \tag{1.71}$$

Chapter Two
Optical Waveguide Sensors

2.1 Introduction

The need for minute instruments (biosensors) to detect or predict diseases or harmful substances has become a must. Intensive research has been conducted on developing biosensors in the past few decades and have resulted great improvements. Optoelectonics played an essential part in these improvements. Especially optical techniques have proven interesting features for biosensing due to the possibility of rapid, direct (unlabeled) detection [8].

2.2 Slab Waveguide Optical Sensors

Optical waveguides were primarily developed for telecommunication purposes. In 1983 Teifenthelar and Lukosz, who are the fathers of slab waveguide sensors, proved the applicability of a dielectric slab waveguide as an optical sensor. They were studying a waveguide with grating coupler and discovered changes in coupling angles due to variations of humidity. Since then waveguide sensor systems have been the subject to a large number of investigations which led to an enormous advance in the field and many techniques have been developed. In this dissertation, evanescent field sensing will be studied.

2.2.1 Definition and Principle of Work

An optical biosensor is simply a device that forces light to interact with the measurand (specimen) and then converts the light signal affected/perturbed by the measurand into a readable electric signal, which carries the necessary information about the measurand or the process under investigation.

As mentioned before the guided wave inside the core is associated with an evanescent field in the surrounding layers. This decaying field penetrates and interacts with the cladding as shown in Fig. 2.1. Changing the refractive index of the cladding will change the effective index of the guide. As a result the coupled mode will be changed and can be realized by a change in intensity, phase, polarization, frequency, emission or reflection [9].

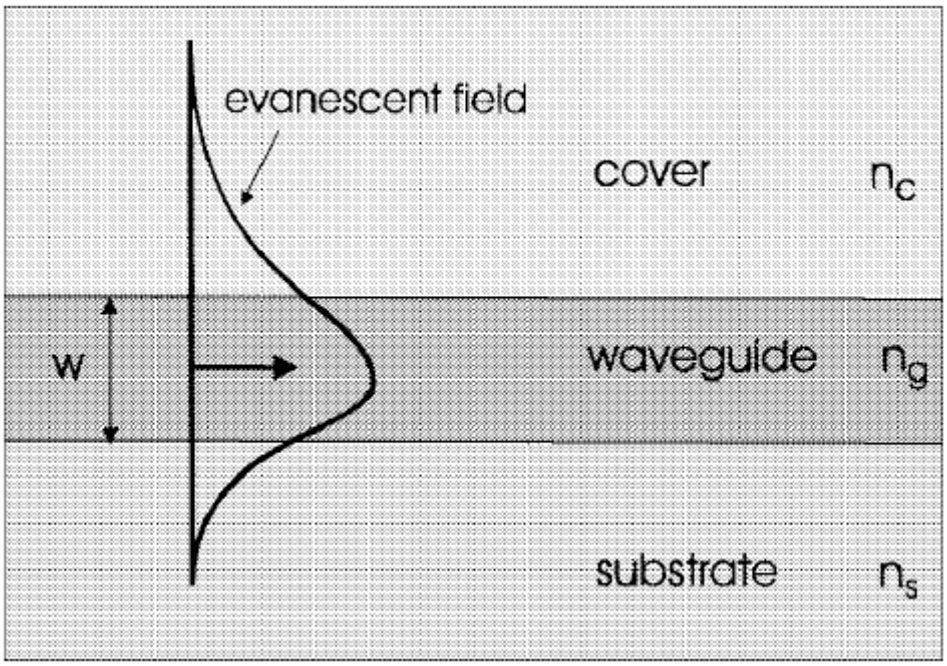

Fig. 2.1. Schematic illustrating of an evanescent field penetrating the cover and substrate layers.

Evanescent field sensing can be applied to several different transduction approaches including evanescent fluorescence detection, monitoring of refractive index changes or detecting spectroscopic shifts [8].

2.2.2 Advantages of Optical Sensors:

Slab waveguide sensors have a wide range of applications, some of them can be summarized as follows:

1- Detecting the existence and/or concentrations of dangerous gases and liquids.

2- Sensing bacteria and viruses.

3- Monitoring biochemical reactions.

4- Sensing Explosives.

5- Monitoring humitdity.

6- Estimating blood glucose levels.

7- Industrial applications.

Optical slab waveguide sensors have very important characteristics which make them more competitive than other sensing techniques [10-13]:

- Rapid response.
- Direct (unlabelled) detection.
- Immunity to electromagnetic interference.
- Small size/weight.
- Resistance to chemically aggressive and ionizing environments.
- Easy to interface with optical data communication systems and secure data transmission.
- High sensitivity.
- Low cost.

2.2.3 Classification

Optical sensors can be classified from different aspects. For example they can be classified according to the role of the waveguide into extrinsic or intrinsic sensors [9]. In extrinsic sensors the waveguide is used to transport light to and from the sensing region, i.e. sensing is done outside the waveguide. While in intrinsic sensors, both transportation of light and sensing is done inside the waveguide. Figure 2.2 shows the configuration of both types.

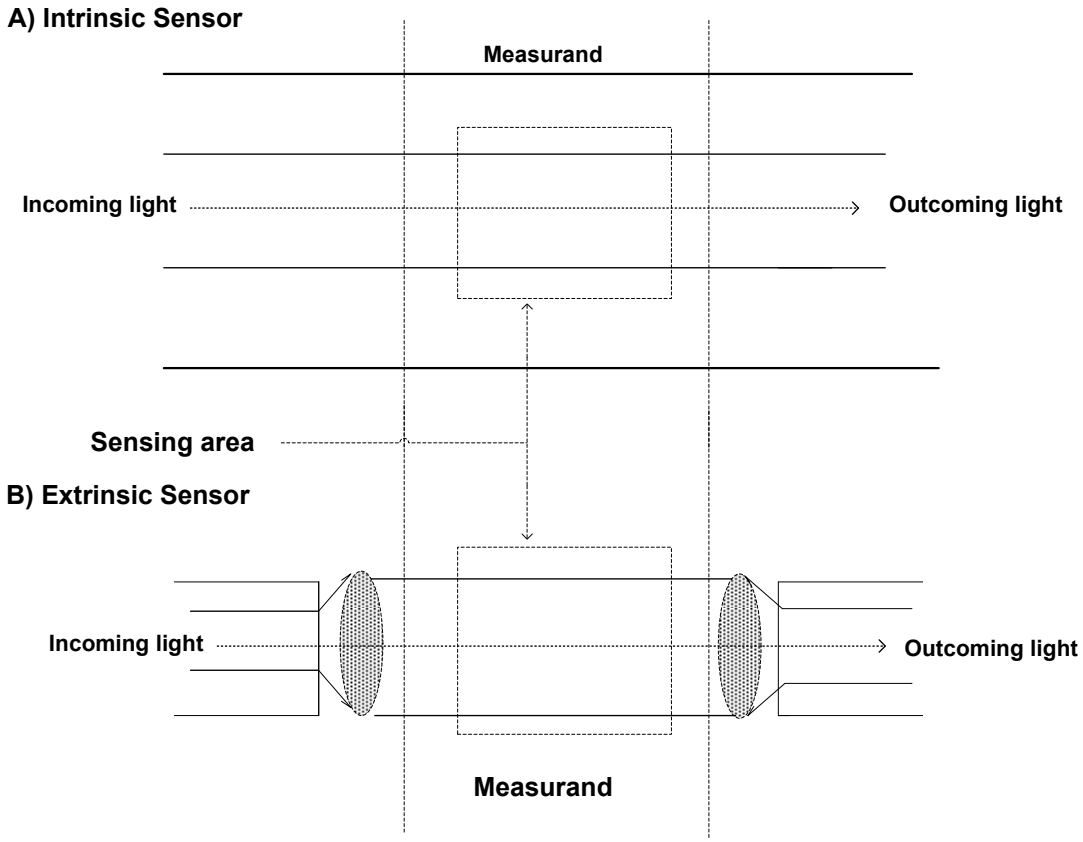

Fig. 2.2. Illustration of the difference between intrinsic and extrinsic sensors.

Another way to classify optical sensors is the number of coupled modes used in the sensing process into single mode and multimode sensors. The waveguide in single mode sensors is very thin film with thickness comparable to the operating wavelength. While in multimode sensors, the waveguide thickness is much greater than the operating wavelength. H. Mukundan et. al. [8], made a comprehensive review on both types.

Labeled or unlabeled sensing is another important aspect to classify sensors. It is also called homogeneous or surface(inhomogeneous) sensing. Label free sensors have the structure shown in Fig. 2.1., where the measurand is homogeneously distributed on the sensor surface. While in surface sensors an

additional thin layer is added above the core. It usually an affinity layer that binds the measurnad to the sensor surface forming what's called an adlayer. This layer is usually a fluorescent, enzymes, radioactive or other type of materials. Fig. 2.3. shows a schematic for a surface sensor.

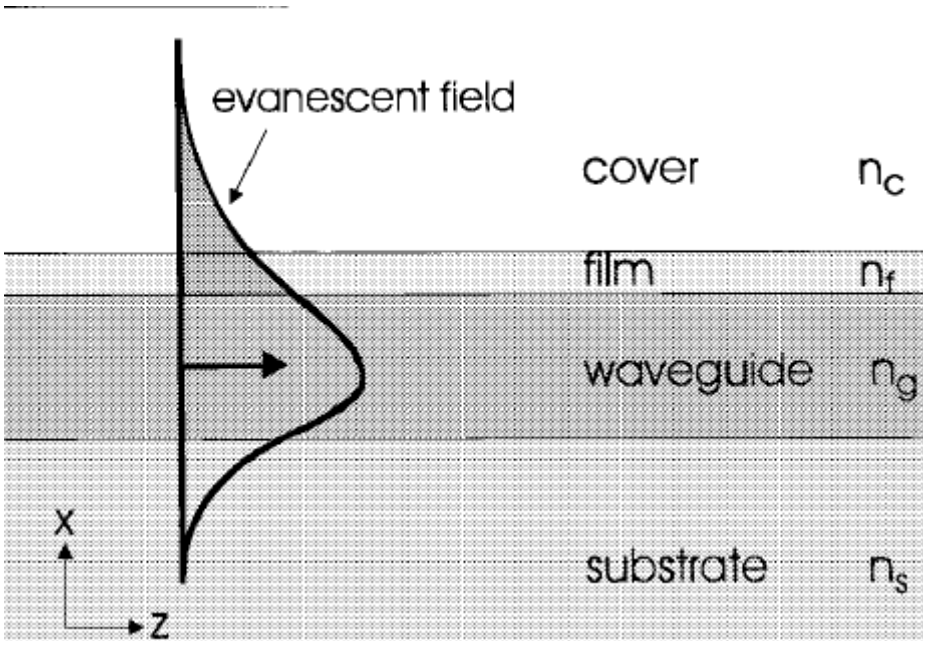

Fig. 2.3. Schematic representation of a surface sensor.

Label free sensing enable numerous experiments and biochemical investigations such as protein/protein or protein/small molecule binding [14]. It is essential in this case not to use a label since it may affect the interaction. Label free sensing is related to the sample concentration or surface density, instead of total sample mass. As a result, the detection signal does not scale down with the sample volume [15]. Label free sensing saves resources and time since it does not need further treatment.

The advantage of surface sensing is that it gives specificity and more flexibility to the investigation of biochemical molecules resulting in an almost limitless domain for the discovery and understanding of biochemical interactions [16].

Label-free detection removes experimental uncertainty induced by the effect of the label on molecular conformation, blocking of active binding epitopes, steric hindrance, inaccessibility of the labeling site, or the inability to find an appropriate label that functions equivalently for all molecules in an experiment. Label-free detection methods greatly simplify the time and effort required for assay development while removing experimental artifacts from quenching, shelf life, and background fluorescence[17].

2.2.4. Sensor Sensitivity

The effective index of the guided mode depends on the structure parameters, i.e. the refractive indices of the three layers and the thickness of the guiding layer. The evanescent field of the guided mode penetrates both the substrate and cover layers. Any change in the cover index will change the effective index of the guided mode, this is the sensing criteria. Mathematically the sensitivity *S* of a homogeneous sensor is given by

$$S_{n_c} = \frac{\partial N}{\partial n_c}. \qquad (2.1)$$

For surface sensors the sensitivity is defined as the change of the effective index due to the change in the adlayer's thickness d_A or refractive index n_A as [18] ,

$$S_{d_A} = \frac{\partial N}{\partial d_A} \quad \text{or} \quad S_{n_A} = \frac{\partial N}{\partial n_A} \ . \qquad (2.2)$$

Increasing the interaction of the evanescent field with the cover increases the sensitivity. In other words, maximizing the field strength at the film/cover interface and the penetration depth is the key to maximize the sensitivity [8].
For a specific detection or measurement using a slab waveguide sensor, the sensitivity can be maximized by

1- Proper choice of the film and substrate layers.

2- Proper choice of the coupled mode.

3- Proper adlayer might be added.

4- Adding extra layers.

5- Changing the magnetic or electric characteristics of the waveguide, as will be seen in this thesis.

2.3 Previous Work

Evanescent field sensing has captured great attention due to its advantages. Since the discovery of Teifenthelar and Lukosz, hundreds of researches on the subject and many structures and techniques were introduced. It is now well established and sensor systems have been developed and demonstrated by numerous investigators. Studies on slab waveguide sensors have concentrated on enhancing the resolution, miniaturizing the whole system, lowering the cost, and mainly maximizing the sensor sensitivity.

H. Mukundan et al. [8] described the basic principles, advantages and disadvantages of planar optical waveguide based biodetection technologies. This discussion included already commercialized technologies and new technologies that are under research and development. Moreover, they discussed reverse-symmetry waveguides, resonant waveguide grating sensors and metal-clad leaky waveguides as alternative signal transducers in optical biosensing.

Two types of operation for metal-clad waveguides have been analyzed: peak-type and dip-type operation were presented in details in Ref. [10]. The newly discovered peak-type operation was obtained by use of thin claddings (a few nanometers) between the substrate and the film that consist of metals with a large imaginary permittivity, whereas dip-type operation was obtained by use of thicker claddings (some tens of nanometers) of metals with small imaginary permittivity.

An overview about a wide range of sensor transducers was presented in Ref. [14]. The working principles and the peculiarities of each technology, e.g., concerning the set-up, sensitivity, sensor size or required sample volume are discussed.

The recent progress in optical biosensors that use the label-free detection protocol, in which biomolecules are unlabeled, was reviewed in Ref. [15]. The paper focused on the optical biosensors that utilize the refractive index change as the sensing transduction signal. Various optical label-free biosensing platforms were introduced, including surface plasmon resonance, interferometers, waveguides, fiber gratings, ring resonators, and photonic crystals.

Parruiaux et al. [19] derived analytically the conditions for maximum sensitivity for both transverse electric (TE) and transverse magnetic (TM) evanescent-wave step-index waveguide sensors. The analysis covered both cases where the measurand is homogeneously distributed in the semi-infinite waveguide cover, and where it is an ultrathin film at the waveguide-cover interface. El-Agez et al. [20] have investigated the variation of the sensitivity of optical slab waveguide sensors with the wavelength of the guided wave. They found that an optimum wavelength exists for each guiding layer thickness and this optimum value increases linearly with the thickness of the guiding layer. Taya et al. [21] proposed two pioneer sensors based on Fabry-Perot resonator and fringes of equal thickness structure. Different from the conventional slab waveguide sensors in which the sample interacts with the evanescent field in the cladding layer, the proposed sensors in Ref 21 contain the sample in the core layer. The first proposed sensor comprises a piezoelectric material as a substrate with the driving potential difference as the sensing probe for refractive index changes of the sample. The second sensor comprises fringes of equal thickness structure with the number of fringes per unit length is the probe for changes in the index of the sample. Skivesen et al [22], analyzed metal-clad waveguides for sensor applications to achieve high sensitivity for adlayer and refractive index measurements. Their optimization

showed that it is possible for metal-clad waveguides to achieve a sensitivity improvement up to 6 times compared to surface-plasmon-resonance sensors. Taya et al. [23-26] proposed optical waveguide sensors in which one or both of the surrounding media have an intensity dependent refractive index. In these articles, an extensive theoretical analysis of slab waveguide sensors comprising self-focusing and self-defocusing nonlinear media was presented. The sensitivity was derived when the effective index is greater and smaller than the refractive index of the guiding layer. The behavior of the sensitivity with different parameters of the structure was presented. Closed form analytical expressions and normalized charts were given to provide the conditions for the maximum sensitivity of nonlinear sensors when the measurand is homogeneously distributed in the
semi-infinite waveguide cover. The results were compared with those of the well known linear evanescent waveguide sensors. It is found that utilizing nonlinear media can enhance the sensitivity of slab waveguide sensors. Another class of optical waveguide sensors has been proposed with the so-called reverse symmetry design [27-29]. In these structures the substrate has a refractive index being less than that of the cladding medium. This design offers deeply penetrating evanescent optical fields into the analyzed cover sample. Therefore, the sensitivity has shown an improvement in the reverse symmetry configuration. In Ref. 29, an extensive theoretical treatment of an optical waveguide sensor consisting of thin dielectric film surrounded by an aqueous cladding and an ideal nonabsorbing plasma substrate was presented. The authors considered the case when the frequency of the guided light is greater than the plasma frequency so that the refractive index of the substrate is less than unity. This structure provides a reverse symmetry configuration in which the refractive index of the substrate is less than that of the cladding. The sensitivity of the effective index of the proposed structure to changes in the refractive index of the aqueous cladding was studied with different parameters of the structure. The results showed considerable enhancement of the sensitivity compared to the conventional optical waveguide structure with

normal symmetry using a glass substrate. The effect of the plasma substrate on the Goos-Hanchen shift, on the effective index of structure, and on the power flow in the waveguide structure was investigated.

Left-handed materials (LHMs) of simultaneously negative dielectric permittivity ε and magnetic permeability μ have been studies in the field of optical waveguide sensors [30-35]. It was verified that LHMs can amplify evanescent waves. Therefore, slab waveguide structures comprising LHMs are expected to improve the sensitivity of waveguide sensors. The sensitivity of an optical waveguide sensor was shown to be dramatically enhanced by using a LHM layer between the guiding layer and the covering medium [30]. Planar three-layer waveguide consisting of thin left handed material core layer was investigated for sensing applications [32]. The sensitivity of the proposed sensor to the changes in the refractive index of the cladding and the power confinement factor in each layer were presented. It was found that the sensitivity of the proposed structure is negative and critically dependent on the frequency dependent ε and μ of the left handed material core layer. A four-layer waveguide structure comprising a dielectric substrate, a metal layer, a left-handed material (LHM) as a guiding layer, and a cladding was investigated as a metal-clad waveguide sensor [34]. Fresnel reflection coefficients were used to study the resonance dips at which the reflectance minimizes. The simulation showed that the proposed structure has a preference over the surface plasmon resonance structure since it gives much sharper reflectance dip and can achieve considerable sensitivity improvement. A symmetric three-layer slab waveguide with a left handed material as a guiding layer was examined analytically for cover refractive index detection [35]. The TM mode dispersion relation and the sensitivity of the proposed waveguide were investigated. The sensitivity improvement compared with the conventional three-layer waveguide sensor was approximately a factor of 6.

Previous researchers studied different structures of waveguide sensors, they changed the properties of the layers (for example LHM or nonlinear material) constituting the waveguide or added new layers (thin metal or LHM layers)

and studied the effect on the sensitivity. In this thesis, another approach is discussed. Changing the electrical characteristics of the waveguide and its effect on the modal field is studied. This is done by adding a surface conductivity at the interfaces of a dielectric waveguide i.e. the film/cover and film/substrate interfaces, solving ME's for the new structure, and deriving the dispersion relation and the sensitivity to variations of the cover's refractive index.

Chapter Three
Three-layer Slab Waveguide Optical Sensor with Conductive Interfaces: TE case

In this chapter, three-layer slab waveguide structure is considered for sensing applications. Surface charge is assumed at the substrate/film and film/cover interfaces. The dispersion relation, sensitivity, power flow relations are derived, plotted and analyzed.

3.1 Introduction

Khorasani et al. [36] presented a dielectric slab waveguide with conducting interfaces. They studied the waveguide analytically for TE and TM modes. They concluded that such a waveguide may be used as a modulator or a switch by controlling a transverse voltage. They suggested that such a structure has potential applications in the technology of integrated optical computing.

In this thesis another application is studied. A theoretical study of a similar waveguide as an optical sensor is conducted. This chapter is dedicated to the study of TE modes in such waveguide sensor. The dispersion relation, sensitivity and the time-average power flowing in the three layers are derived.

3.2 Dispersion Relation

Fig. 3.1. shows a schematic diagram of the slab waveguide structure under consideration. It consists of a thin film of high refractive index having parameters (ε_f, μ_f) and thickness d, deposited on a less denser substrate with parameters (ε_s, μ_s), and a cladding at the top of the sensor with parameters (ε_c, μ_c) which represents the sample to be tested.

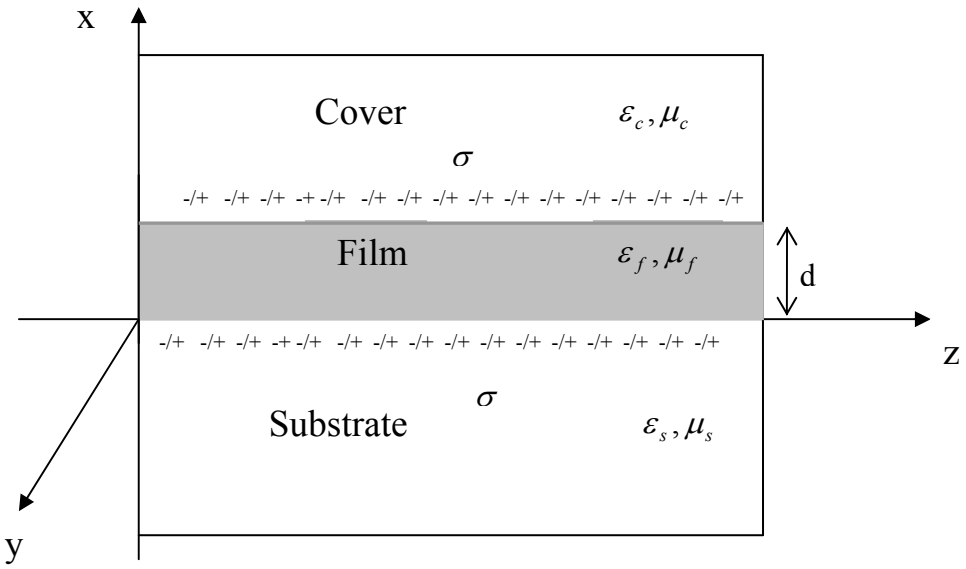

Fig. 3.1. A schematic of three-layer slab waveguide with conducting interfaces.

As mentioned in chapter 1, the only nonzero components of TE mode are E_y, H_x and H_z. Rewriting Maxwell's equations in three dimensions, taking into account the conductivity σ on the two interfaces,

$$\begin{vmatrix} \hat{i} & \hat{j} & \hat{k} \\ \partial/\partial x & \partial/\partial y & \partial/\partial z \\ 0 & E_y & 0 \end{vmatrix} = -i\mu\omega(H_x\hat{i} + H_y\hat{j} + H_z\hat{k}), \qquad (3.1)$$

and

$$\begin{vmatrix} \hat{i} & \hat{j} & \hat{k} \\ \partial/\partial x & \partial/\partial y & \partial/\partial z \\ H_x & 0 & H_z \end{vmatrix} = i\varepsilon\omega(E_x\hat{i} + E_y\hat{j} + E_z\hat{k}) + \sigma(E_x\hat{i} + E_y\hat{j} + E_z\hat{k}). \quad (3.2)$$

Eq. (3.1) gives

$$H_x = -\frac{\beta}{\omega\mu} E_y , \tag{3.3}$$

$$H_z = -\frac{1}{i\omega\mu} \frac{\partial E_y}{\partial x} , \tag{3.4}$$

whereas Eq. (3.2) gives

$$(i\omega\varepsilon + \sigma) E_y = \frac{\partial H_x}{\partial x} - \frac{\partial H_z}{\partial z} . \tag{3.5}$$

Substituting Eqs. (3.3) and (3.4) into Eq. (3.5) yields,

$$(i\omega\varepsilon + \sigma) E_y = \frac{1}{i\omega\mu} \frac{\partial^2 E_y}{\partial x^2} - \frac{\beta^2}{i\omega\mu} E_y . \tag{3.6}$$

From which the TE wave equation can be written as

$$\frac{\partial^2 E_y}{\partial x^2} + (\omega^2 \varepsilon\mu - \beta^2 - i\omega\mu\sigma) E_y = 0 . \tag{3.7}$$

The above equation is Helmholtz equation for TE polarized light in a slab waveguide with conducting interfaces. It is clear that Eq. (3.7) reduces to Eq. (1.52) when $\sigma = 0$. The solution of Eq. (3.7) in the three layers is given by

$$E_y(x) = \begin{cases} Ae^{-\alpha_c (x-d)}, x > d \\ B_1 \cos(\alpha_f x) + B_2 \sin(\alpha_f x), 0 < x < d \\ Ce^{\alpha_s x}, x < 0 \end{cases} , \tag{3.8}$$

where A, B_1, B_2 and C are coefficients representing the wave amplitudes in the three layers and the parameters α_c, α_f and α_s have different forms from those given be Eqs. (1.54)-(1.56). They now have the forms

$$\alpha_c = (\beta^2 - k_0^2 n_c^2 + i\omega\mu_c\sigma)^{1/2}, \tag{3.9}$$

$$\alpha_f = (k_0^2 n_f^2 - \beta^2 - i\omega\mu_f\sigma)^{1/2}, \tag{3.10}$$

and

$$\alpha_s = (\beta^2 - k_0^2 n_s^2 + i\omega\mu_s\sigma)^{1/2}. \tag{3.11}$$

Consequently, the nonzero magnetic field components can be written as

$$H_x(x) = -\frac{\beta}{\omega}\begin{cases} \dfrac{A}{\mu_c} e^{-\alpha_c(x-d)} : x > d \\ \dfrac{1}{\mu_f}(B_1\cos(\alpha_f x) + B_2\sin(\alpha_f x)) : 0 < x < d \\ \dfrac{C}{\mu_s} e^{\alpha_s x} : x < 0 \end{cases}, \tag{3.12}$$

$$H_z(x) = -\frac{1}{i\omega}\begin{cases} \dfrac{-\alpha_c}{\mu_c} A e^{-\alpha_c(x-d)} : x > d \\ \dfrac{\alpha_f}{\mu_f}(-B_1\sin(\alpha_f x) + B_2\cos(\alpha_f x)) : 0 < x < d \\ \dfrac{\alpha_s}{\mu_s} C e^{\alpha_s x} : x < 0 \end{cases}. \tag{3.13}$$

Applying the boundary conditions at x = 0 and x = d, the dispersion relation can be derived as

$$\alpha_f d = \tan^{-1}\gamma_{cTE} + \tan^{-1}\gamma_{sTE} + m\pi, \tag{3.14}$$

where

$$\gamma_{cTE} = \frac{\mu_f}{\alpha_f}\left(\frac{\alpha_c}{\mu_c} - i\omega\sigma\right), \tag{3.15}$$

and

$$\gamma_{sTE} = \frac{\mu_f}{\alpha_f}\left(\frac{\alpha_s}{\mu_s} - i\omega\sigma\right). \tag{3.16}$$

Again, γ_{cTE} and γ_{sTE} reduce to their values given by Eq. (1.58) when $\sigma = 0$.

3.3 Sensitivity of the structure

For homogeneous sensing, the sensitivity of the effective refractive index to the variation of the cover's index is given by Eq. (2.1), namely,

$$S = \frac{\partial N}{\partial n_c}. \tag{3.17}$$

To find a mathematical expression for S, the dispersion relation given by Eq. (3.14) is differentiated with respect to *N*. We get,

$$S = \frac{\mu_f n_c}{\mu_c \alpha_c N}\left(\left[d + \frac{\mu_f}{1+\gamma_{sTE}^2}\left\{\frac{1}{\alpha_s\mu_s} + \frac{\gamma_{sTE}}{\mu_f\alpha_f}\right\}\right] + \frac{1}{1+\gamma_{cTE}^2}\left\{\frac{\mu_f}{\alpha_c\mu_c} + \frac{\gamma_{cTE}}{\alpha_f}\right\}\right)^{-1}, \tag{3.18}$$

where γ_{cTE} and γ_{sTE} are given by Eqs. (3.15) and (3.16).

3.4 Power Flow

The time-average power flowing in the three layers of the waveguide is given by Eq. (1.65). Making use of the three equations giving E_y in the three layers (Eq. (3.8)), we get

$$P_s = \frac{\beta}{2\omega\mu_s}\int_{-\infty}^{0}\left|Ce^{\alpha_s x}\right|^2 dx = \frac{\beta}{4\omega\mu_s\alpha_s}C^2, \tag{3.19}$$

$$P_c = \frac{\beta}{2\omega\mu_c}\int_{d}^{\infty}\left|Ae^{-\alpha_c(x-d)}\right|^2 dx = \frac{\beta}{4\omega\mu_c\alpha_c}A^2, \tag{3.20}$$

and

$$P_f = \frac{\beta}{2\omega\mu_f}\int_{0}^{d}\left|B_1\cos\alpha_f x + B_2\sin\alpha_f x\right|^2 dx,$$

$$P_f = \frac{\beta}{4\omega\mu_f}\left[d\left(B_1^2+B_2^2\right)+\frac{1}{\alpha_f}\cos\left(\alpha_f d\right)\sin\left(\alpha_f d\right)\left(B_1^2-B_2^2\right)+\frac{B_1B_2}{\alpha_f}\sin\left(\alpha_f d\right)\right] \tag{3.21}$$

The coefficients A, B_1, B_2 and C are connected to each other through the boundary conditions. It is found that

$$B_1 = C, \tag{3.22}$$

$$B_2 = \frac{\mu_f}{\alpha_f}\left(\frac{\alpha_s}{\mu_s}-i\omega\sigma\right)C, \tag{3.23}$$

and

$$A = \left[\cos\left(\alpha_f d\right)+\frac{\mu_f}{\alpha_f}\left(\frac{\alpha_s}{\mu_s}-i\omega\sigma\right)\sin\left(\alpha_f d\right)\right]C. \tag{3.24}$$

The total power flowing in the proposed waveguide structure can be obtained by summing the power in all layers

$$P_{total} = P_f + P_c + P_s. \tag{3.25}$$

The sensitivity of slab waveguides to any change in the index of the cover layer is critically dependent on the fraction of total power flowing in the cover.

3.5 Results and Discussion

In the following analysis the following parameters are used, He-Ne laser beam of λ_0 = 632.8 nm is assumed to be guided in one of two types of films: the first is an SiO_2-TiO_2 film (WG1) with parameters ε_f = 3.0625 and μ_f = 1 (n_f = 1.75) and the second is an Si_3N_4 film (WG2) of parameters ε_f = 4.0401 and μ_f = 1 (n_f = 2.01), the measurand is assumed to be water of parameters ε_c = 1.77 and μ_c =1 (n_c = 1.33) or air of parameters ε_c = 1 and μ_c = 1 (n_c = 1), and pyrex glass substrate with n_s = 1.47 and μ_s = 1 (ε_s = 2.1609) for both waveguides.

The dispersion relation given by Eq. (3.14) is solved numerically using a MAPLE 9 code for the propagation constant β. When β is obtained for a waveguide configuration, the sensitivity of the effective refractive index to any variation in the cover refractive index is calculated. Following the above procedure Figs. 3.2-3.9 were plotted using four different values of σ [36].

Fig. 3.2 shows the sensitivity of the proposed sensor for SiO_2-TiO_2 guiding film and water cladding. The solid line shows the behavior of the sensitivity with the guiding layer thickness for the conventional three-layer slab waveguide sensor with no conducting interfaces. There exists an optimum value of the film thickness at which the sensitivity is maximum. This thickness is slightly above the cutoff thickness at which the effective index is equal to that of the substrate layer and the sensitivity is zero, because all the wave propagates in the substrate and no evanescent field is present in the cladding. Therefore, the wave does not feel any changes in the cladding index. For thicknesses larger than the optimum thickness, the sensitivity decays due to the high confinement of the wave in the relatively thick guiding layer and the reduction in the evanescent tail.

When conductivity is introduced at the substrate/film and film/cladding interfaces, the sensitivity curve versus the film thickness has the same shape as that of non conductive interfaces with a clear enhancement in the sensitivity, specially at the optimum thickness. Moreover, as the conductivity σ increases, the maximum sensitivity increases and the curve peak gets sharper. For σ = 0, the maximum sensitivity is found to be about 23% whereas for $\sigma = i50\times10^{-7}/\eta_0$ the maximum sensitivity becomes about 37%, which can be considered a considerable enhancement. Another feature that can be observed from Fig. 3.2 is the shift of the optimum thickness towards higher values as σ increases.

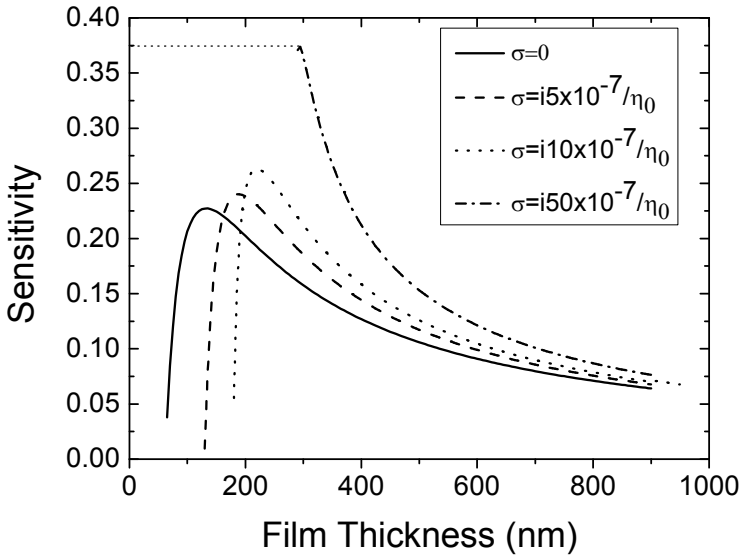

Fig. 3.2 Sensitivity of the proposed waveguide structure versus film thickness for the fundamental mode TE_0 and different values of σ for ε_f=3.0625 (SiO_2-TiO_2), ε_s=2.1609, λ_0 =632.8nm and water in the cladding layer (ε_c=1.77).

The sensitivity versus the film thickness of SiO_2-TiO_2 film is shown in Fig. 3.3 for air cover layer. The behavior of the sensitivity is exactly similar to that of the water analyte structure with smaller values in the case of air cover. The maximum sensitivity when σ = 0 is 11% and it becomes 17% when $\sigma = i50\times10^{-7}/\eta_0$. The sensitivity in this case is lower than that in Fig. 3.2

because the ratio $\frac{n_c}{n_f}$ of the water analyte structure is greater than that of the air analyte structure.

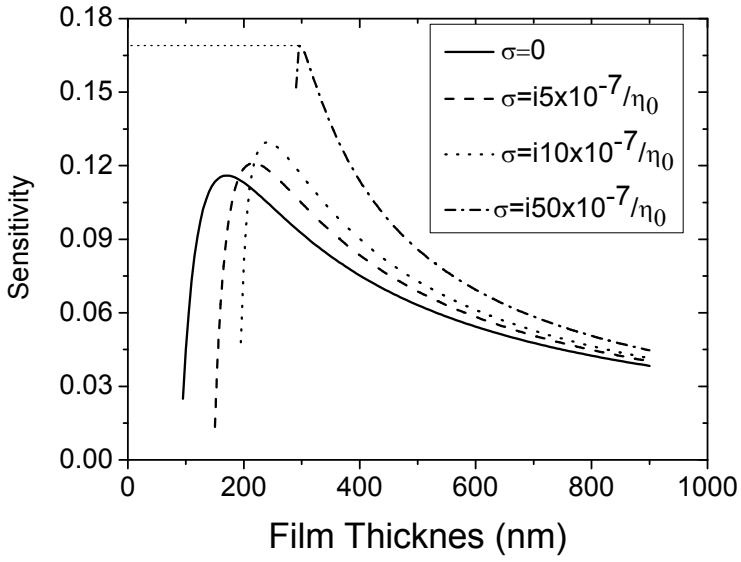

Fig. 3.3 Sensitivity of the proposed waveguide structure versus film thickness for the fundamental mode TE_0 and different values of σ for ε_f=3.0625 (SiO_2-TiO_2), ε_s=2.1609, λ_0 =632.8nm and air in the cladding layer (ε_c=1).

To study the effect of changing the refractive index of the guiding layer on the sensitivity, Figs. 3.4 and 3.5 are plotted for a guiding film with larger refractive index, an Si_3N_4 film (ε_f = 4.0401). It is obvious that the sensitivity increased for both water and air claddings. Using a conductivity of $\sigma = i50 \times 10^{-7} / \eta_0$, in the water cladding case, gives a sensitivity of more than 47% for WG2 (Fig. 3.4) compared to 37% for WG1 (Fig. 3.2). While using the same conductivity for air cladding gives a sensitivity of about 22% for WG2 (Fig. 3.5) compared to 17% for WG1 (Fig. 3.3). This increase in the sensitivity between the two structures is a result of the difference n_f - n_s and not because of n_f itself. This result is in agreement with the work of other researchers [37].

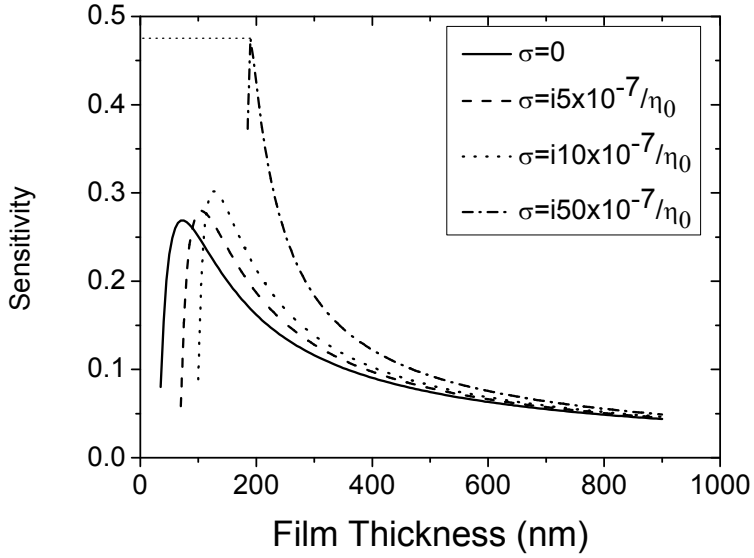

Fig. 3.4 Sensitivity of the proposed waveguide structure versus film thickness for the fundamental mode TE_0 and different values of σ for ε_f=4.0401 (Si_3N_4), ε_s=2.1609, λ_0 =632.8nm and water in the cladding layer (ε_c=1.77).

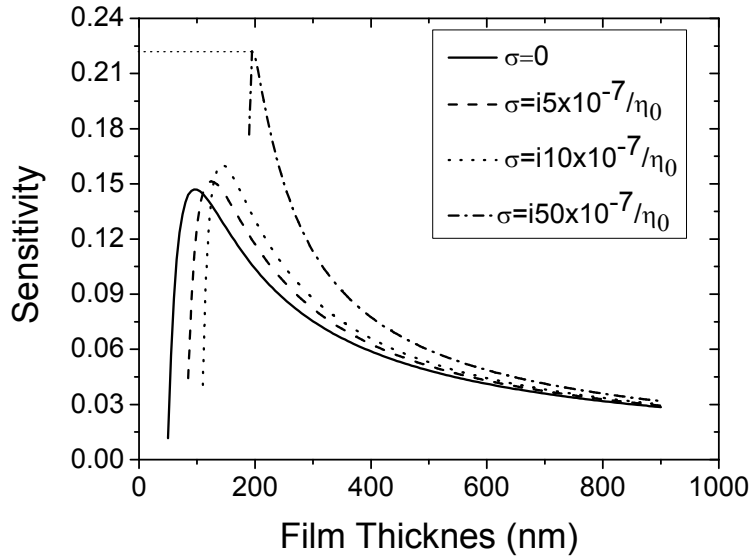

Fig. 3.5 Sensitivity of the proposed waveguide structure versus film thickness for the fundamental mode TE_0 and different values of σ for ε_f=4.0401 (Si_3N_4), ε_s=2.1609, λ_0 =632.8nm and air in the cladding layer (ε_c=1).

The sensitivity of the first mode TE_1 is now investigated for both waveguides. Figs. 3.6 - 3.9 are plotted for water and air claddings for both WG1 and WG2 waveguides. Figure 3.6 shows the sensitivity versus the guiding film thickness for SiO_2-TiO_2 film and water analyte in the cladding whereas Fig. 3.7 shows the same film with air analyte. The sensitivities of the Si_3N_4 guiding film are shown in Fig. 3.8 for water in the cladding and Fig. 3.9 for air in the cladding. As expected, the sensitivity has lower values than those of the fundamental mode TE_0. The explanation for that is the film thickness is larger for TE_1 than that of TE_0 which means the wave is more confined and the evanescent field in the cladding is smaller for TE_1. Increasing the conductivity still enhances the sensitivity. For example, assuming a conductivity of $\sigma = i50\times10^{-7}/\eta_0$ using WG1 with water analyte increases the sensitivity up to about 20% compared with 13.7% for σ = 0 as illustrated in Fig. 3.6 which means an enhancement of more than 45%. The values of S are still smaller when using the same structure with air cladding (Fig. 3.7).

When using Si_3N_4 as a guiding layer and water as an analyte the peak reaches 0.26 when $\sigma = i50\times10^{-7}/\eta_0$ compared to 0.17 when $\sigma = 0$ as Fig. 3.8 reveals. Comparing Figs 3.6 and 3.8, there is an improvement in the sensitivity of about 30% for $\sigma = i50\times10^{-7}/\eta_0$ due to using Si_3N_4 film instead of SiO_2-TiO_2 film. In a similar manner, Fig. 3.9 shows a sensitivity enhancement of 33% for $\sigma = i50\times10^{-7}/\eta_0$ when compared to Fig. 3.7. Moreover, Figs. 3.6-3.9 still show the same property of shifting the optimum thickness to higher values as the surface conductivity increases.

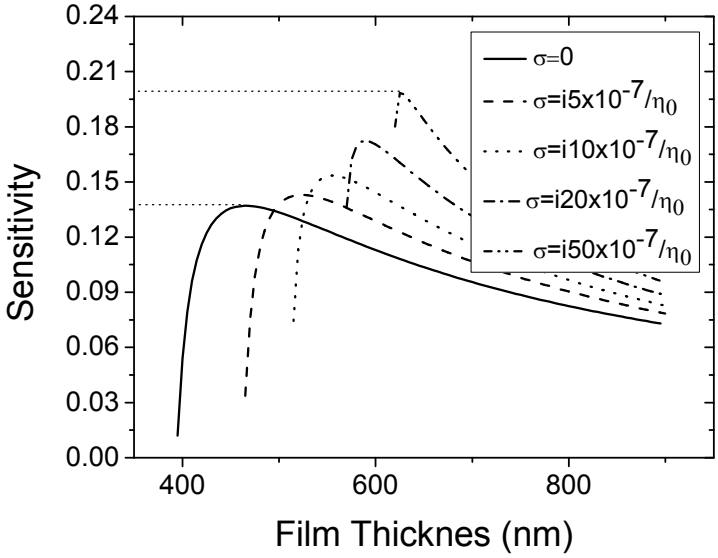

Fig. 3.6 Sensitivity of the proposed waveguide structure versus film thickness for the first mode TE_1 and different values of σ for ε_f=3.0625 (SiO_2-TiO_2), ε_s=2.1609, λ_0 =632.8nm, and water in the cladding layer (ε_c=1.77).

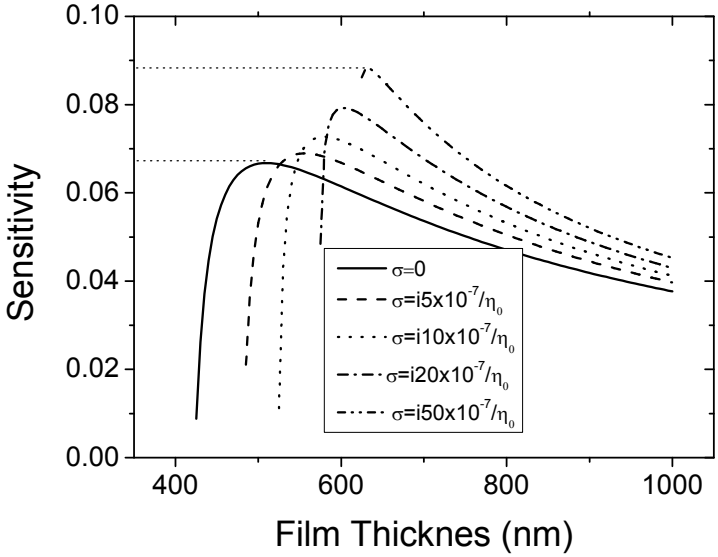

Fig. 3.7 Sensitivity of the proposed waveguide structure versus film thickness for the first mode TE_1 and different values of σ for ε_f=3.0625 (SiO_2-TiO_2), ε_s=2.1609, λ_0 =632.8nm and air in the cladding layer (ε_c=1).

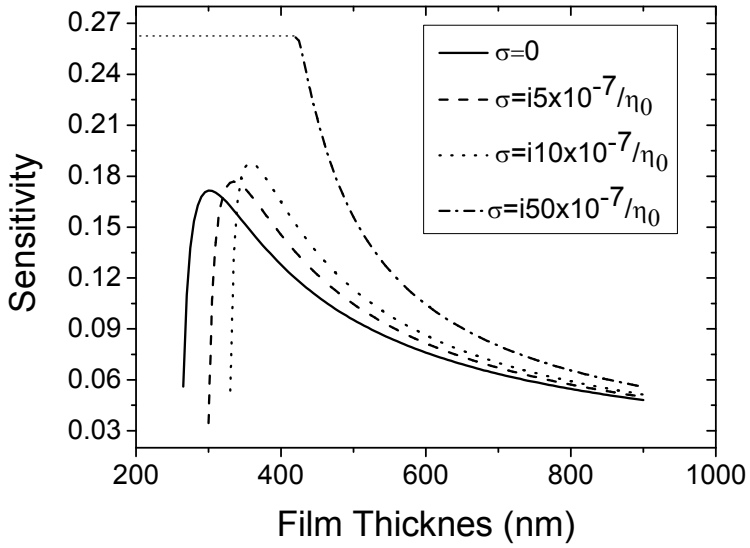

Fig. 3.8 Sensitivity of the proposed waveguide structure versus film thickness for the first mode TE_1 and different values of σ for ε_f=4.0401 (Si_3N_4), ε_s=2.1609, λ_0 =632.8nm and water in the cladding layer (ε_c=1.77).

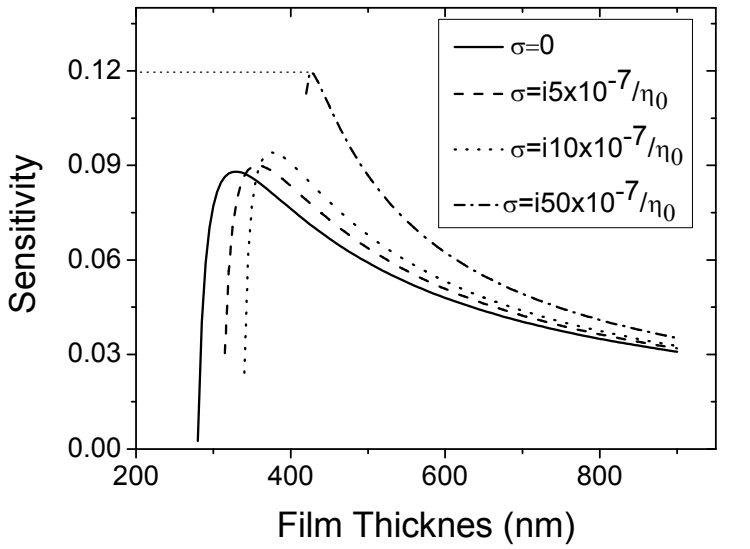

Fig. 3.9 Sensitivity of the proposed waveguide structure versus film thickness for the first mode TE_1 and different values of σ for ε_f=4.0401 (Si_3N_4), ε_s=2.1609, λ_0 =632.8nm and air in the cladding layer (ε_c=1).

The most important feature of the proposed sensor is the sensitivity enhancement in the presence of the conducting interfaces. It is obvious from Figs. 3.2-3.9 that increasing the conductivity enhances the sensitivity. In Figs. 3.2-3.9, the calculations were restricted to charge densities in the range $\sigma = 0$ to $\sigma = i50 \times 10^{-7} / \eta_0$. In Fig. 3.10, the sensitivity of Si_3N_4 waveguide film and water cladding structure is plotted versus the guiding layer thickness for a wider range of σ values. All features that have been seen in previous figures are still observed in Fig. 3.10. It is also clear from the figure that increasing S with σ is not and an endless process. There exists something like a "saturation limit" after which increasing σ will not give a noticeable increase in the sensitivity.

It can be seen from Figs. 3.2-3.9 that increasing the conductivity at substrate/film and film/cover interfaces increases the optimum thickness at which the sensitivity peaks exist. This is clear from the shift of the sensitivity curves to the right towards larger values of film thicknesses. This shift increases as the conductivity increases. However, the above discussion regarding the limit is also applicable here, i.e. there exists a saturation value of σ after which the curve shift is negligible.

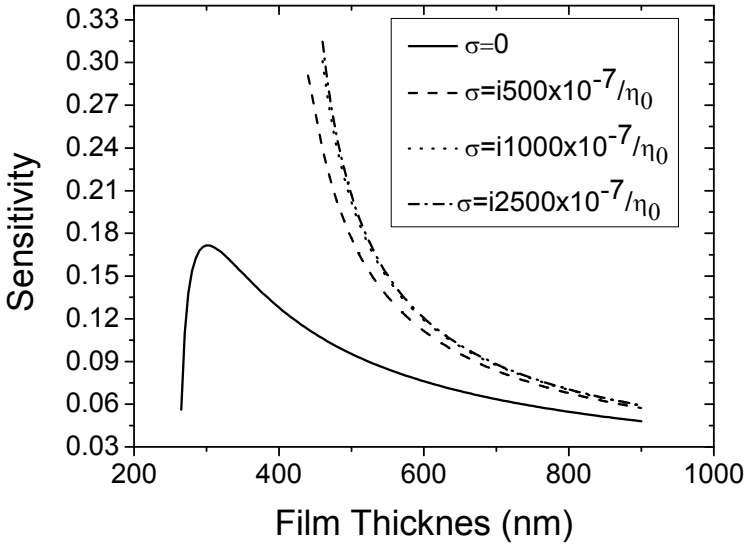

Fig. 3.10 Sensitivity of the proposed waveguide structure versus film thickness for the first mode TE_1 and high values of σ for ε_f=4.0401 (Si_3N_4), ε_s=2.1609, λ_0 =632.8nm and water in the cladding layer (ε_c=1.77).

Figs. 3.2-3.10 were plotted for the proposed sensor using positive conductivity. To complete the picture, Figs. 3.11-3.18 are plotted for the sensitivity versus film thickness using a negative conductivity for the above waveguide configurations. Fig. 3.11 shows the sensitivity of SiO_2-TiO_2 film and water analyte for TE_0 mode for negative values of the conductivity density whereas Fig. 3.12 shows the same for air analyte. The behavior of the sensitivity with the guiding layer thickness for Si_3N_4 film is illustrated in Fig. 3.13 for water and Fig. 3.14 for air for the negative values of σ.

It is clear from Figs. 3.11-3.14 that the addition of negative conductivity to the interfaces of the sensor also increases the sensitivity. On the other hand, increasing the negative conductivity shifts the optimum thickness towards lower values and hence decreases the cutoff thickness. This makes a limit for the amount of the surface charge that can be added specially when utilizing the fundamental mode. As a result it is not possible to use high surface conductivity.

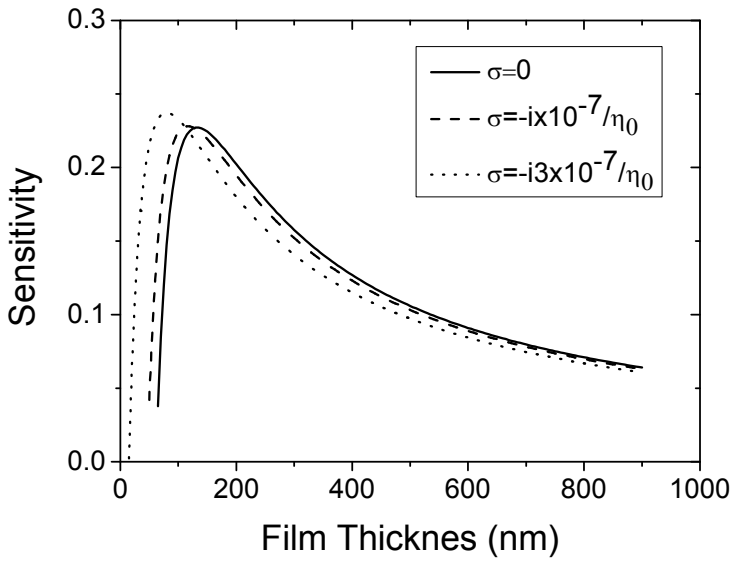

Fig. 3.11 Sensitivity of the proposed waveguide structure versus film thickness for the fundamental mode TE_0 and negative values of σ for ε_f=3.0625 (SiO_2-TiO_2), ε_s=2.1609, λ_0 =632.8nm and water in the cladding layer (ε_c=1.77).

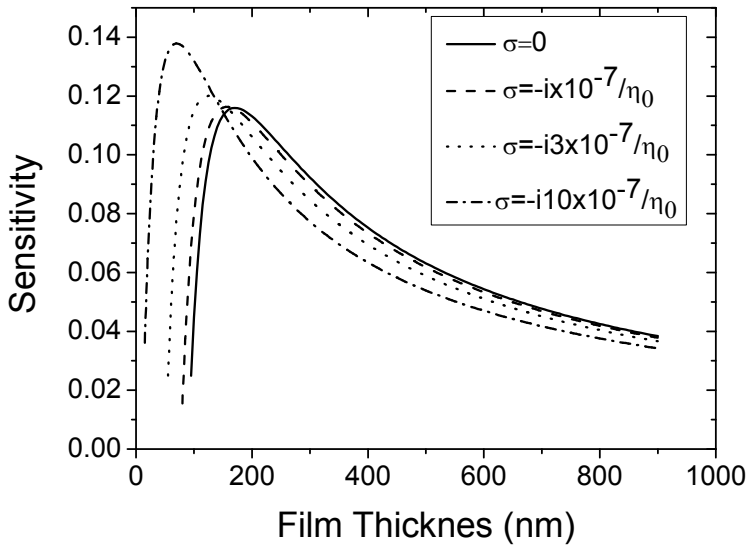

Fig. 3.12 Sensitivity of the proposed waveguide structure versus film thickness for the fundamental mode TE_0 and negative values of σ for ε_f=3.0625 (SiO_2-TiO_2), ε_s=2.1609, λ_0 =632.8nm and air in the cladding layer (ε_c=1).

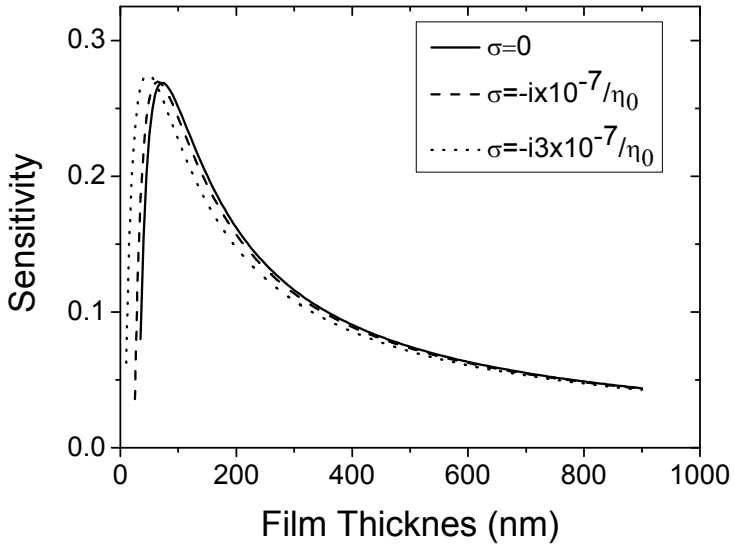

Fig. 3.13 Sensitivity of the proposed waveguide structure versus film thickness for the fundamental mode TE_0 and negative values of σ for ε_f=4.0401 (Si_3N_4), ε_s=2.1609, λ_0 =632.8nm and water in the cladding layer (ε_c=1.77).

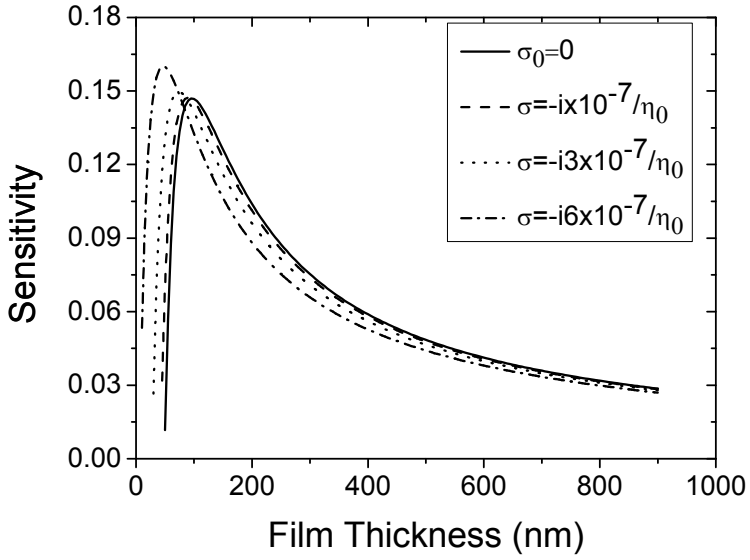

Fig. 3.14 Sensitivity of the proposed waveguide structure versus film thickness for the fundamental mode TE_0 and negative values of σ for ε_f=4.0401 (Si_3N_4), ε_s=2.1609, λ_0 =632.8nm and air in the cladding layer (ε_c=1).

It is worth to investigate the dependence of the sensitivity on negative charge density for higher mode orders. Compared to the fundamental mode, the first mode occurs at lager thicknesses of the guiding film. Therefore the curve shift towards thinner film thicknesses will keep both the optimum and cutoff thicknesses at practically accepted values. Moreover, it is possible to consider high values of negative charge at the interfaces to obtain relatively considerable sensitivity enhancement. The sensitivities of TE_1 mode for WG1 and WG2 and both water and air analytes are shown in Figs. 3.15-3.18. Significant sensitivity improvement can be seen in these figures compared with Figs. 3.11-3.14.

For example, the addition of a conductivity of $\sigma = -i15\times10^{-7}/\eta_0$ to the first waveguide with water cladding, gave a sensitivity of about 0.337 compared to 0.137 for the normal sensor $\sigma = 0$ (Fig. 3.15) which gives a sensitivity enhancement of about 150%. While adding the same conductivity to same waveguide with air analyte gives a sensitivity of about 0.135 compared to about 0.067 when $\sigma = 0$ (Fig. 3.16). This means an enhancement of more than 100%.

Fig. 3.17 shows the sensitivity versus the film thickness using different negative values of σ at the interfaces of WG2 with water as a cladding for TE_1. Using $\sigma = -i20\times10^{-7}/\eta_0$ gives a sensitivity of about 0.395 compared to 0.17 for the conventional sensor ($\sigma = 0$). Moreover, the same charge density for air at the cover layer (Fig. 3.18) gives a sensitivity of 0.184 compared to 0.089 for $\sigma = 0$. Again the sensitivity improvement is more that 100% in both cases.

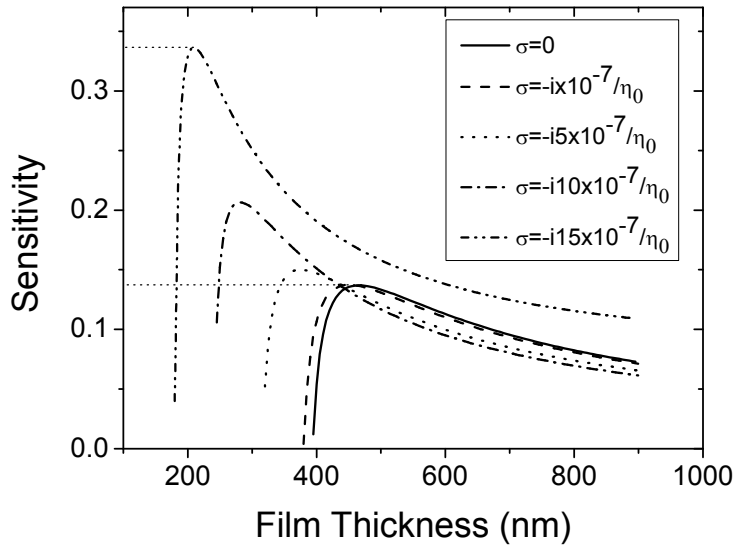

Fig. 3.15 Sensitivity of the proposed waveguide structure versus film thickness for the first mode TE_1 and negative values of σ for ε_f=3.0625 (SiO_2-TiO_2), ε_s=2.1609, λ_0 =632.8nm and water in the cladding layer (ε_c=1.77).

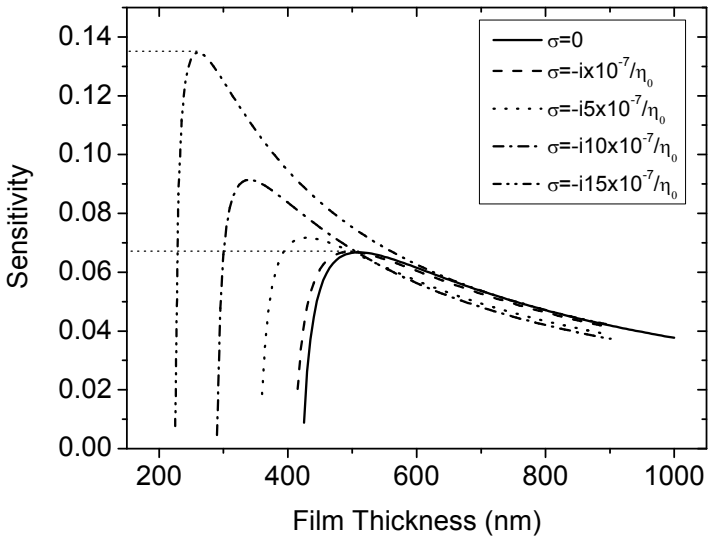

Fig. 3.16 Sensitivity of the proposed waveguide structure versus film thickness for the first mode TE_1 and negative values of σ for ε_f=3.0625 (SiO_2-TiO_2), ε_s=2.1609, λ_0 =632.8nm and air in the cladding layer (ε_c=1).

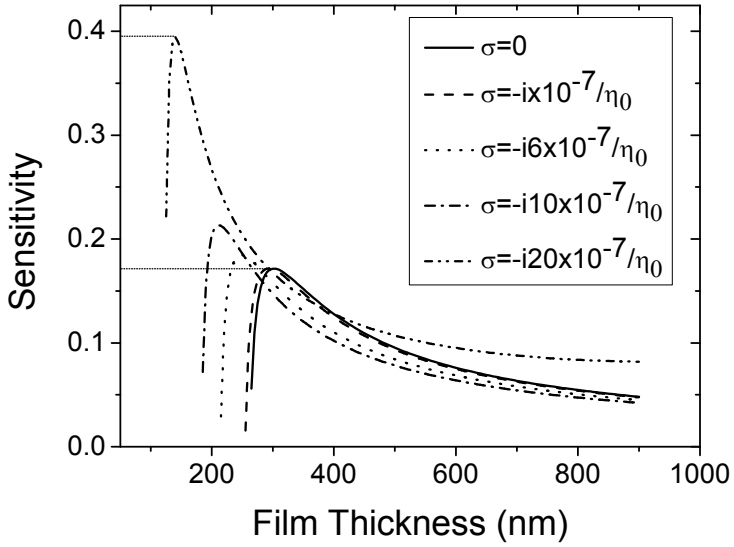

Fig. 3.17 Sensitivity of the proposed waveguide structure versus film thickness for the first mode TE_1 and negative values of σ for ε_f=4.0401 (Si_3N_4), ε_s=2.1609, λ_0 =632.8nm and water in the cladding layer (ε_c=1.77).

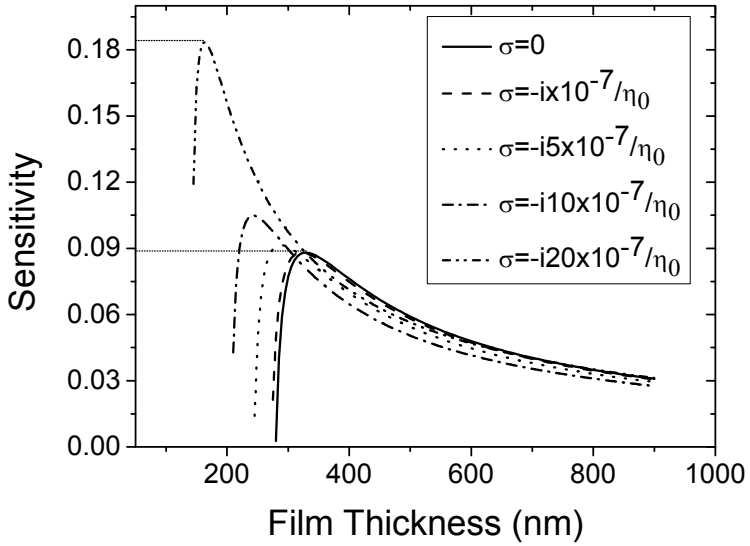

Fig. 3.18 Sensitivity of the proposed waveguide structure versus film thickness for the first mode TE_1 and negative values of σ for ε_f=4.0401 (Si_3N_4), ε_s=2.1609, λ_0 =632.8nm and air in the cladding layer (ε_c=1).

Strange peaks in the sensitivity curves were obtained when using higher negative conductivity as shown in Fig. 3.19. Very high values of sensitivity at the optimum thickness were obtained in the figure for extreme possible values of negative conductivity. These peaks need to be studied or experimented carefully. If confirmed, it would be a tremendous enhancement in the sensitivity.

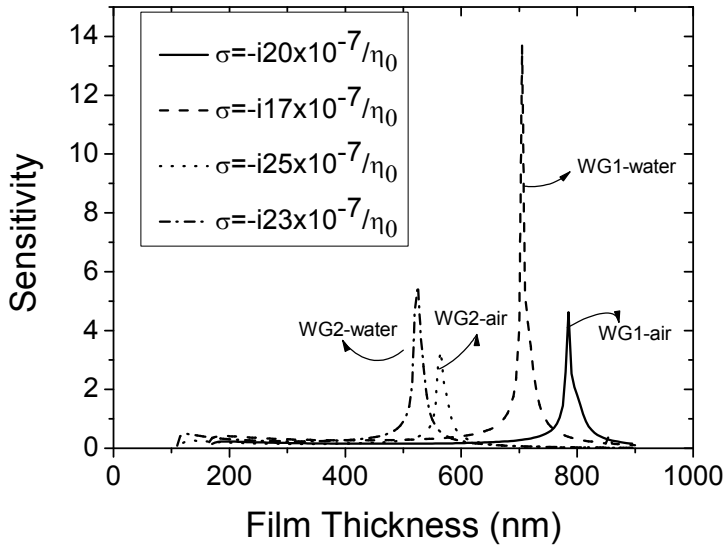

Fig. 3.19 Sensitivity versus film thickness for the first mode TE_1 and large negative values of σ for WG1 and WG2 for air and water in the cladding layer.

As mentioned earlier, the principle of optical sensors is that the evanescent tail interacts with the cover. The larger the tail is, the more interaction with the cladding occurs as a result greater sensitivity is obtained. Larger evanescent field means more power flowing in the cladding. It is constructive to study the time-average power flowing in the cladding for our proposed sensor. Using Eq. (3.20), Fig. 3.19 is plotted for the power flowing in the cladding. It shows a comparison between the time-average power for the proposed sensor for four

different values of conductivity. When using conductivity $(\sigma = i5\times10^{-7}/\eta_0)$ the time-average power flowing in the cover is two times larger than that of the traditional waveguide. While using $(\sigma = i50\times10^{-7}/\eta_0)$ increased the power flowing in the cover about ten times larger. It is concluded that the enhancement of the sensitivity obtained in all previous figures is obviously attributed to the increase of the power flowing in the cladding.

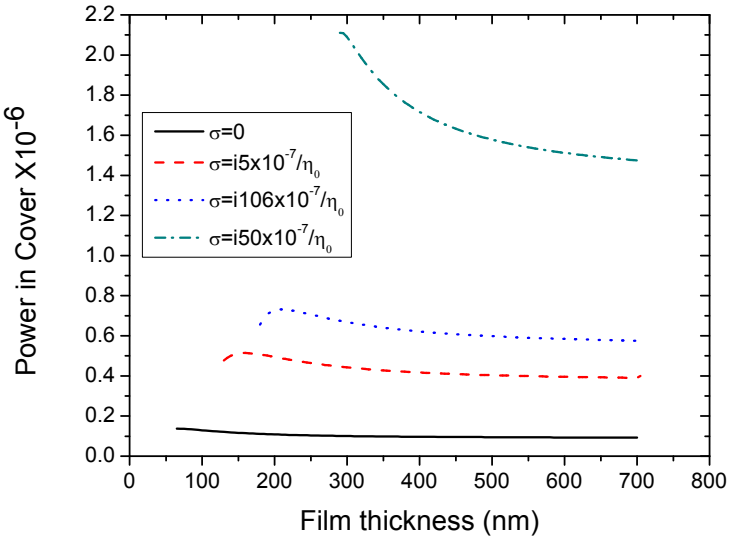

Fig. 3.20 Power flowing in the cover versus film thickness for the fundamental mode TE_0 and positive values of σ for WG1: parameters ε_f=3.0625, ε_s=2.1609 and λ_0=632.8nm and water in the cladding layer.

Chapter Four
Three-layer Slab Waveguide Optical Sensor with Conducting Interfaces: TM case

In this chapter, TM polarized light is assumed to propagate in a slab waveguide with conducting interfaces. The structure is treated as an optical waveguide sensor for homogeneous sensing applications. Transverse resonance condition for TM modes is derived. Moreover, the sensitivity of the effective index to any variation in the index of an analyte is presented.

4.1 Dispersion Relation

The same three-layer waveguide structure shown in Fig. 3.1 is still considered. The guided waves are assumed to have p-polarization (TM). The nonzero components in TM mode are H_y, E_x and E_z. From Eq. (3.2),

$$E_x = -\frac{i\beta}{i\omega\varepsilon + \sigma} H_y, \tag{4.1}$$

and

$$E_z = \frac{1}{i\omega\varepsilon + \sigma} \frac{\partial H_y}{\partial x}. \tag{4.2}$$

The y-component of Eq. (3.1) is given by

$$-i\mu\omega H_y = \frac{\partial E_x}{\partial z} - \frac{\partial E_z}{\partial x}. \tag{4.3}$$

Substituting for E_x and E_z from Eqs. (4.1) and (4.2) into Eq. (4.3) yeilds

$$\frac{\partial^2 H_y}{\partial x^2} + (\omega^2 \varepsilon\mu - \beta^2 - i\omega\mu\sigma) H_y = 0 . \qquad (4.4)$$

The last equation is the wave equation for TM polarized light is a slab waveguide with conducting interfaces. The solution of Eq. (4.4) for H_y in the three layers of the waveguide structure is given by

$$H_y(x) = \begin{cases} ae^{-\alpha_c(x-d)}, x > d \\ b_1 \cos(\alpha_f x) + b_2 \sin(\alpha_f x), 0 < x < d \\ ce^{\alpha_s x}, x < 0 \end{cases}, \qquad (4.5)$$

where a, b_1, b_2 and c are constants giving the wave amplitudes in the three layers. They can be determined from the boundary conditions. The parameters α_c, α_f and α_s are still given by Eqs. (3.9)-(3.11).

In p-polarization, the electric field has two nonzero components. They can be determined using Eqs. (4.1) and (4.2).

$$E_x(x) = \begin{cases} \frac{i\beta}{i\omega\varepsilon_c + \sigma} ae^{-\alpha_c(x-d)} : x > d \\ \frac{i\beta}{i\omega\varepsilon_f + \sigma} (b_1 \cos(\alpha_f x) + b_2 \sin(\alpha_f x)) : 0 < x < d \\ \frac{i\beta}{i\omega\varepsilon_s + \sigma} ce^{\alpha_s x} : x < 0 \end{cases}, \qquad (4.6)$$

$$E_z(x) = \begin{cases} \frac{-\alpha_c}{i\omega\varepsilon_c + \sigma} ae^{-\alpha_c(x-d)} : x > d \\ \frac{\alpha_f}{i\omega\varepsilon_f + \sigma} (-b_1 \sin(\alpha_f x) + b_2 \cos(\alpha_f x)) : 0 < x < d \\ \frac{\alpha_s}{i\omega\varepsilon_s + \sigma} ce^{\alpha_s x} : x < 0 \end{cases}. \qquad (4.7)$$

The continuity requirement at the interfaces gives the following dipersion relation

$$\alpha_f d = \tan^{-1}\gamma_{cTM} + \tan^{-1}\gamma_{sTM} + m\pi\,, \tag{4.8}$$

where,

$$\gamma_{cTM} = (\frac{\alpha_c}{\alpha_f}\frac{i\omega\varepsilon_f + \sigma}{i\omega\varepsilon_c + \sigma})(1 - \frac{\sigma\alpha_c}{i\omega\varepsilon_c + \sigma})^{-1}\,, \tag{4.9}$$

and

$$\gamma_{sTM} = (\frac{\alpha_s}{\alpha_f}\frac{i\omega\varepsilon_f + \sigma}{i\omega\varepsilon_s + \sigma})(1 - \frac{\sigma\alpha_s}{i\omega\varepsilon_s + \sigma})^{-1}. \tag{4.10}$$

It should be noted that all above equations reduce to equations in subsection (1.2.3.2), when $\sigma = 0$.

4.2 Sensitivity

We are interested in the sensitivity of the guided mode to any changes in the refractive index of the analyte. The sensitivity is still given by the change in the effective refractive index of the guided mode due to any change in the analyte index as in the TE case. Eq. (4.8) is now differentiated with respect to N to get $\frac{\partial n_c}{\partial N}$ and then the sensitivity is calculated as $\left(\frac{\partial n_c}{\partial N}\right)^{-1}$.

After tedious mathematical manipulations, the following equation has been obtained for the sensitivity of the proposed structure when TM waves are considered,

$$S = \frac{n_c}{k_0^2 N(1+\gamma_{cTM}^2)(\alpha_f U_c)^2}\left[\alpha_f U_c k_0^2 + \frac{2i\omega\alpha_c\alpha_f}{\mu_c} + \alpha_f \sigma k_0^2\right] \times$$

$$\left[\frac{d}{V\alpha_f} + \frac{(\alpha_f U_c/\alpha_c + \sigma\alpha_f + \alpha_c U_c/\alpha_f)}{(1+\gamma_{cTM}^2)(\alpha_f U_c)^2} + \frac{(\alpha_f U_s + \sigma\alpha_f + \alpha_s U_s/\alpha_f)}{(1+\gamma_{sTM}^2)(\alpha_f U_s)^2}\right]^{-1}, \tag{4.11}$$

where

$$V = i\omega\varepsilon_f + \sigma,$$

$$U_c = i\omega\varepsilon_c + \sigma - \sigma\alpha_c,$$

and

$$U_s = i\omega\varepsilon_s + \sigma - \sigma\alpha_s.$$

4.3 Power Flow

The time-average power flowing in the waveguide structure is given by Eq. (1.71). Substituting for $H_y(x)$ from eq. (4.5) into Eq. (1.71) we get,

$$P_s = \frac{\beta}{2\omega_s\alpha_s}\int_{-\infty}^{0}\left|ce^{\alpha_s x}\right|^2 dx = \frac{\beta}{4\omega\varepsilon_s\alpha_s}c^2, \tag{4.12}$$

$$P_c = \frac{\beta}{2\omega_c\alpha_c}\int_{d}^{\infty}\left|ae^{-\alpha_c(x-d)}\right|^2 dx = \frac{\beta}{4\omega\varepsilon_c\alpha_c}a^2, \tag{4.13}$$

and

$$P_f = \frac{\beta}{2\omega\varepsilon_f}\int_{0}^{d}\left|b_1\cos\alpha_f x + b_2\sin\alpha_f x\right|^2 dx$$

$$= \frac{\beta}{4\omega\varepsilon_f\alpha_f}\left[b_1^2(\alpha_f d + \cos\alpha_f d\sin\alpha_f d) - b_2^2(\cos\alpha_f d\sin\alpha_f d - \alpha_f d) + b_1 b_2\sin^2\alpha_f d\right] \tag{4.14}$$

where the coefficients a, b_1, b_2 and c are related to each other through the relations

$$b_1 = \frac{\alpha_s}{\alpha_f}\left(1 - \frac{\sigma\alpha_s}{i\omega\varepsilon_s + \sigma}\right)c, \tag{4.15}$$

$$b_2 = \frac{\alpha_s}{\alpha_f}\left(\frac{i\omega\varepsilon_f + \sigma}{i\omega\varepsilon_s + \sigma}\right)c \ , \tag{4.16}$$

and

$$a = \frac{\alpha_f}{\alpha_c}\left(\frac{i\omega\varepsilon_c + \sigma}{i\omega\varepsilon_f + \sigma}\right)\left(b_1 \sin\alpha_f d - b_2 \cos\alpha_f d\right). \tag{4.17}$$

4.4 Results and Discussion

The same guiding films used in chapter 3 are still considered here to study the effect of conducting substrate/film and film/ cover interfaces on the sensitivity of the sensor using TM polarized waves. Moreover, the discussion still considers two types of claddings air and water.

MAPLE 9 code was used to solve eq. (4.8) numerically to calculate the propagation constant β. Then the sensitivity was calculated from Eq. (4.11) and plotted.

Fig. 4.1 shows the sensitivity curves for film thicknesses above the cutoff thickness for the first waveguide (WG1) with water analyte, using the fundamental mode TM_0 and positive surface conductivity. It is clear from the figure that introducing a positive surface conductivity at the interfaces reduces the sensitivity, in contrary to the TE case. For a conventional waveguide ($\sigma = 0$) with film thickness d=225nm the sensitivity is 8.5% and when introducing an interface conductivity $\sigma = i0.1\times10^{-7}/\eta_0$ it decreases to 7.4%

and decreases again to 6% when increasing the conductivity up to $\sigma = i0.3\times10^{-7}/\eta_0$.

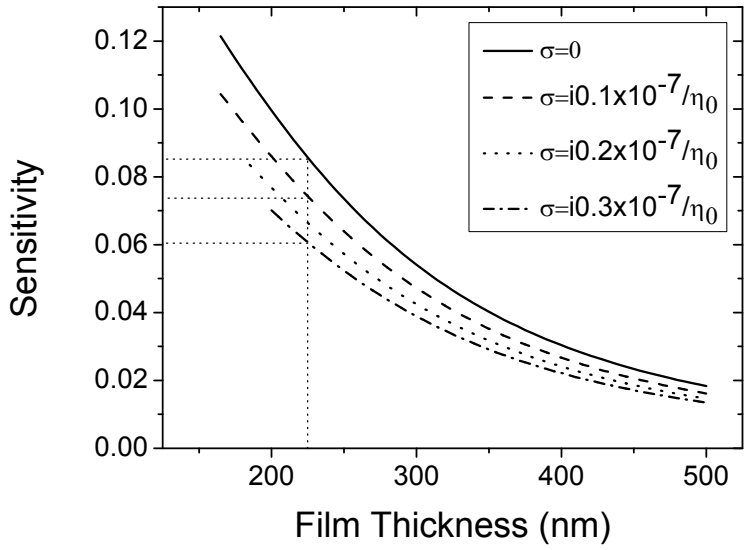

Fig. 4.1 Sensitivity of the proposed waveguide structure versus film thickness for the fundamental mode TM_0 and different values of σ for ε_f=3.0625 (SiO_2-TiO_2), ε_s=2.1609, λ_0=632.8nm and water in the cladding layer (ε_c=1.77).

In Fig. 4.2. the same conductivity values are applied to the same waveguide (WG1) using air as a cover, the sensitivity also decreases as σ increases with even smaller values at the same film thickness (*d*=225nm), which is attributed to the ratio $\frac{n_c}{n_f}$. When $\sigma = 0$ the sensitivity is 8.1%, it decreases to 7% when introducing a surface conductivity of $\sigma = i0.1\times10^{-7}/\eta_0$ and decreases again to 5.7% when increasing the conductivity up to $\sigma = i0.3\times10^{-7}/\eta_0$.

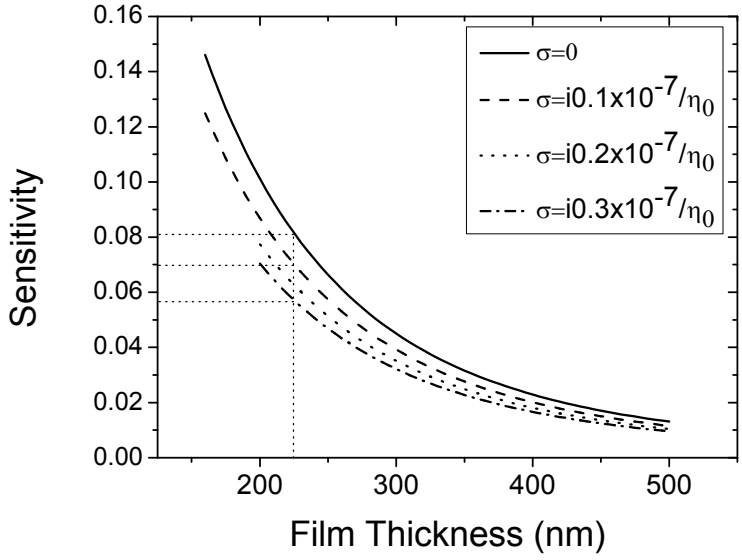

Fig. 4.2 Sensitivity of the proposed waveguide structure versus film thickness for the fundamental mode TM_0 and different values of σ for ε_f=3.0625 (SiO_2-TiO_2), ε_s=2.1609, λ_0 =632.8nm and air in the cladding layer (ε_c=1).

Figs. 4.3 and 4.4 show the sensitivity versus film thickness for WG2 for water and air analytes, respectively for TM_0 mode. Both figures confirm the results obtained in Figs. 4.1 and 4.2. The sensitivity decreases as σ increases. The sensitivity decreases from 9% when σ = 0 to 6.7% for $\sigma = i0.3\times10^{-7}/\eta_0$ when using water in the cover (Fig. 4.3). While it decreases from 7.8% for σ = 0 to 5.6% when $\sigma = i0.3\times10^{-7}/\eta_0$ is added at the interfaces in the air analyte case (Fig. 4.4).

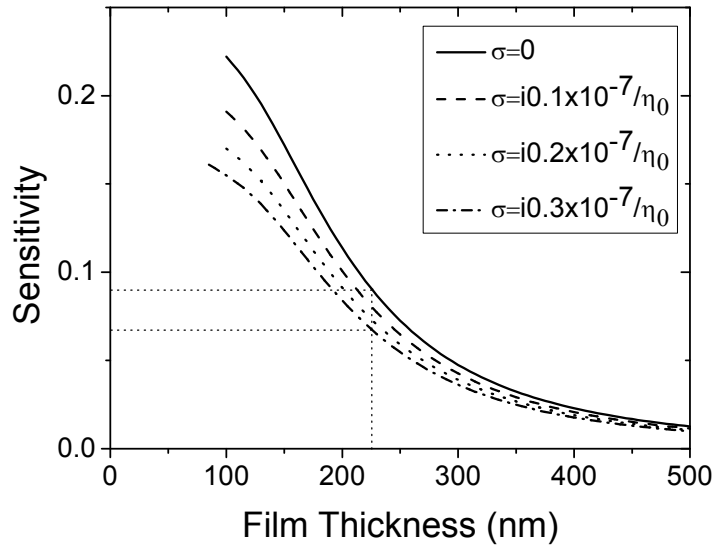

Fig. 4.3 Sensitivity of the proposed waveguide structure versus film thickness for the fundamental mode TM_0 and different values of σ for ε_f=4.0401 (Si_3N_4), ε_s=2.1609, λ_0 =632.8nm and water in the cladding layer (ε_c=1.77).

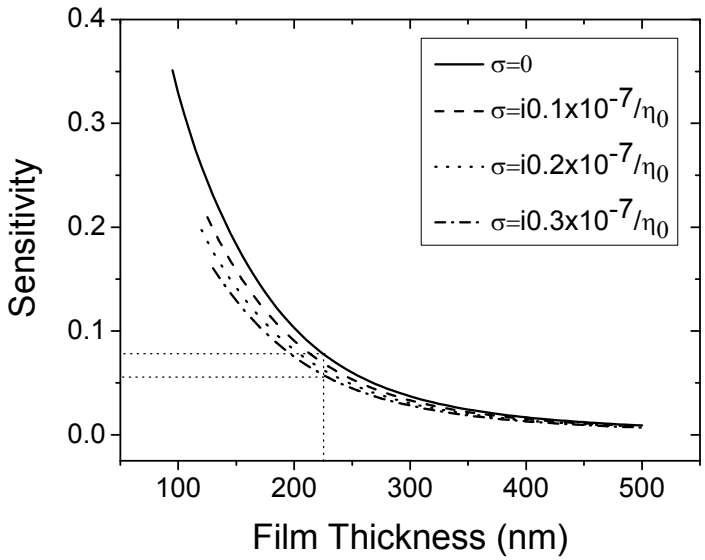

Fig. 4.4 Sensitivity of the proposed waveguide structure versus film thickness for the fundamental mode TM_0 and different values of σ for ε_f=4.0401 (Si_3N_4), ε_s=2.1609, λ_0 =632.8nm and air in the cladding layer (ε_c=1).

It is worth studying the effect of negative surface conductivity the performance of the proposed sensor. Figures 4.5-4.8 were plotted for both waveguides, using water and air in the cover, to study the behavior of the sensitivity when using negative surface conductivity at the interfaces. The results are in agreement with those obtained in the previous chapter in the case of negative surface conductivity. Increasing the surface conductivity enhances the sensitivity.

Figures 4.5 and 4.6 show the behavior of the sensitivity of WG1 for different negative values of σ. At SiO_2-TiO_2 film thickness 200 nm and water cladding, the sensitivity increased from 9.9% for σ = 0 to 17% when employing conducting interfaces of $\sigma = -i0.2\times10^{-7}/\eta_0$ giving an enhancement of about 80% in the sensitivity. At the same film thickness and air cladding, the sensitivity enhancement is 85%, where it increased from 10% for σ = 0 to 18.5% for $\sigma = -i0.2\times10^{-7}/\eta_0$.

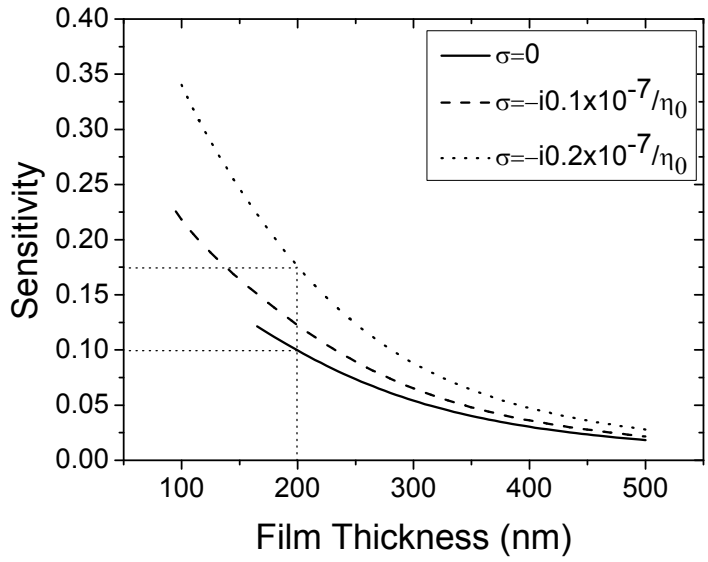

Fig. 4.5 Sensitivity of the proposed waveguide structure versus film thickness for the fundamental mode TM_0 and negative values of σ for ε_f=3.0625 (SiO_2-TiO_2), ε_s=2.1609, λ_0 =632.8nm and water in the cladding layer (ε_c=1.77).

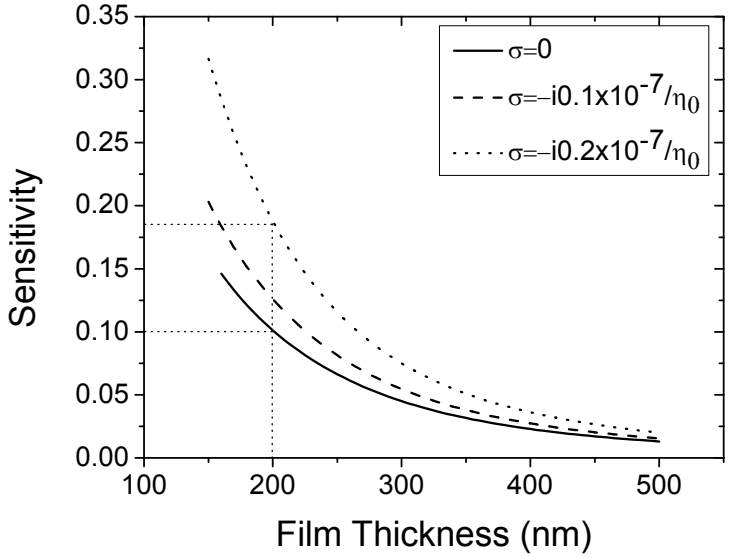

Fig. 4.6 Sensitivity of the proposed waveguide structure versus film thickness for the fundamental mode TM_0 and negative values of σ for ε_f=3.0625 (SiO_2-TiO_2), ε_s=2.1609, λ_0 =632.8nm and air in the cladding layer (ε_c=1).

The same results of Figs. 4.5-4.6 are obtained in Figs. 4.7-4.8 when using WG2 for both claddings. The only difference is the values of the sensitivity are higher in the case of WG2 compared to WG1 which is attributed to the difference n_f- n_s which is larger in WG2.

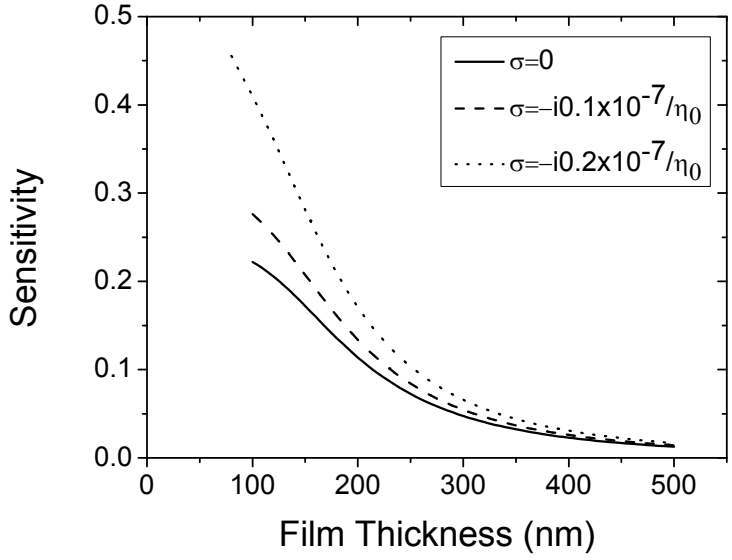

Fig. 4.7 Sensitivity of the proposed waveguide structure versus film thickness for the fundamental mode TM_0 and negative values of σ for ε_f=4.0401 (Si_3N_4), ε_s=2.1609, λ_0 =632.8nm and water in the cladding layer (ε_c=1.77).

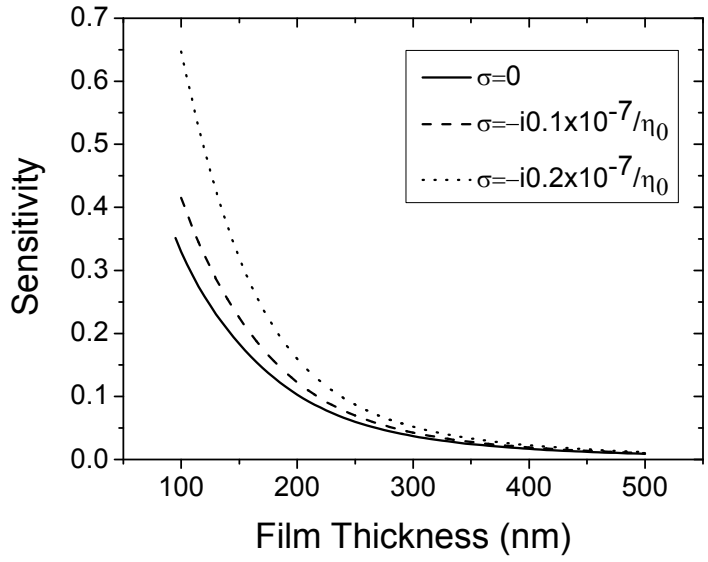

Fig. 4.8 Sensitivity of the proposed waveguide structure versus film thickness for the fundamental mode TM_0 and negative values of σ for ε_f=4.0401 (Si_3N_4), ε_s=2.1609, λ_0 =632.8nm and air in the cladding layer (ε_c=1).

The first mode TM_1 was examined in WG1 and WG2 with water as an analyte. Figures. 4.9-4.12 are plotted to study the behavior of the sensitivity for the first mode for positive as well as negative surface conductivities.

Figs. 4.9 and 4.10 show the sensitivity versus film thickness for both waveguides assuming positive σ. The results agree with results obtained in Figs. 4.1-4.4, for the fundamental mode. It can be concluded that positive surface conductivity at the interfaces reduces the sensitivity of the proposed sensor for TM-modes.

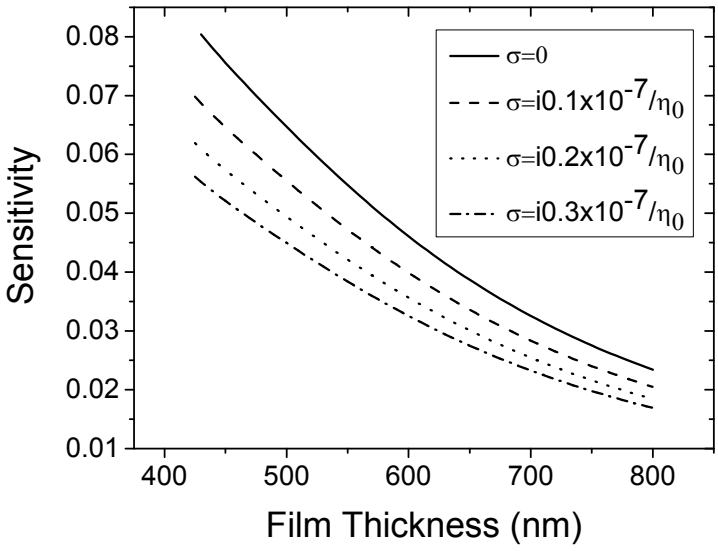

Fig. 4.9 Sensitivity of the proposed waveguide structure versus film thickness for the fundamental mode TM_1 and different values of σ for ε_f=3.0625 (SiO_2-TiO_2), ε_s=2.1609, λ_0 =632.8nm and water in the cladding layer (ε_c=1.77).

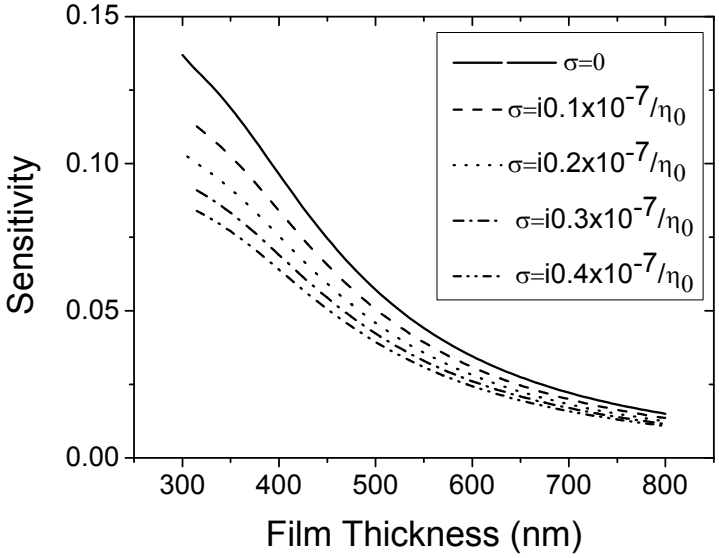

Fig. 4.10 Sensitivity of the proposed waveguide structure versus film thickness for the fundamental mode TM_1 and different values of σ for ε_f=4.0401 (Si_3N_4), ε_s=2.1609, λ_0 =632.8nm and water in the cladding layer (ε_c=1.77).

Finally, the behavior of the sensitivity of TM_1 mode is investigated for WG1 and WG2 in the presence of negative surface conductivity at the interfaces. Figures 4.11 and 4.12 show an improvement of more than 100% when $\sigma = -i0.2\times10^{-7}/\eta_0$ compared to $\sigma = 0$.

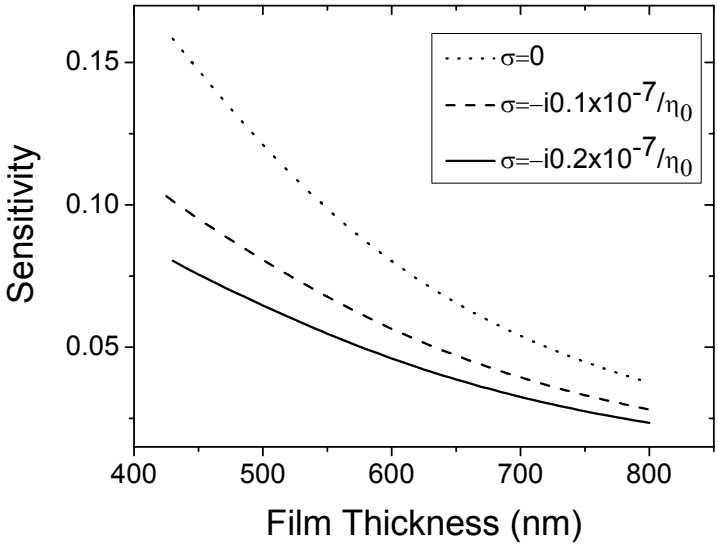

Fig. 4.11 Sensitivity of the proposed waveguide structure versus film thickness for the fundamental mode TM_1 and negative values of σ for ε_f=3.0625 (SiO_2-TiO_2), ε_s=2.1609, λ_0 =632.8nm and water in the cladding layer (ε_c=1.77).

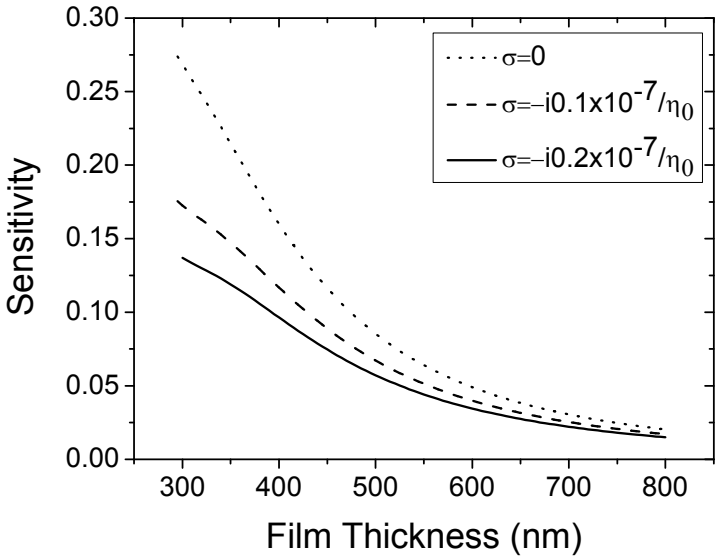

Fig. 4.12 Sensitivity of the proposed waveguide structure versus film thickness for the fundamental mode TM_1 and negative values of σ for ε_f=4.0401 (Si_3N_4), ε_s=2.1609, λ_0 =632.8nm and water in the cladding layer (ε_c=1.77).

Chapter Five
Conclusions

In this thesis, new slab waveguide optical sensor has been proposed. It consists of three dielectric layers with conducting substrate/film and film/cover interfaces. The conducting interfaces can be obtained either by a transverse voltage or by depositing very thin metallic layers between the dielectric layers, of thickness much smaller than that of the wavelength of guided light [36]. The structure has been analyzed for both TE and TM polarized light. The dispersion relations were derived for both polarizations. Expressions for the sensitivity were derived and plotted to study the effect of the surface conductivity on the performance of the sensor, specifically on the sensitivity. Moreover, the effects of positive and negative conductivities were studied on both fundamental and first TE and TM modes. The main results can be summarized as follows:

a) For TE polarized wave

An important advantage of the proposed sensor is the sensitivity enhancement using TE polarized light when utilizing both positive and negative surface conductivities. It was found that adding surface conductivity at the interfaces of a dielectric waveguide increases the sensitivity. It was also noticed that the behavior of the sensitivity of the conducting interface sensor versus the guiding film thickness is identical to that of the conventional waveguide sensor. This was clear from the shape of the sensitivity curves with the guiding film thickness. Using positive as well as negative surface conductivities enhances the sensitivity and makes the sensitivity curve sharper. Another important feature is the saturation level, i.e., for each configuration there exists a certain conductivity value after which there will be no sensitivity enhancement. This was shown for both TE_0 and TE_1 modes. The main

difference between using positive and negative surface conductivities is that increasing σ shifts the sensitivity curve to the right, i.e. to larger film thicknesses, for positive σ while the shift in the case of negative σ towards smaller film thicknesses. This can be explained as an increase or decrease in the cut-off thickness when using positive and negative conductivities, respectively. Moreover, another difference was noticed for TE_1, increasing σ gives better results when using negative conductivity than using positive conductivity. Higher values of sensitivity were obtained when utilizing TE_1 mode and negative conductivity than using positive conductivity and TE_0. Extremely high sensitivity was obtained at high values of negative conductivity and TE_1 mode as shown in Fig. (3.19). If this is confirmed, it would be a breakthrough in the field.

b) For TM polarized wave

The proposed structure was studied using TM polarized light. The obtained results were opposite to those obtained for TE polarized light in the case of positive surface conductivity. The sensitivity of the proposed sensor was less than that of the conventional waveguide sensor and reduces when increasing σ. When negative surface conductivity was used, the results came contrary to the positive surface conductivity and agree with the TE case. The sensitivity of the proposed sensor is greater than the sensitivity of the conventional sensor and it increases as surface conductivity increases.

Future Work

In the future, the following points can be investigated:

- Metal Clad Waveguide (MCWG) structure with conducting interfaces as an optical sensor.
- Peak-type MCWG as well as dip-type MCWG can be studied.
- Multi-layer structure with conducting interfaces as an optical sensor.

- Slab waveguide structure as a surface sensor for adlayer detection.

References

[1] M. Born, M.A. Phill, E. Wolf, "Principles of Optics", 7th edition, Cambridge University Press, UK (2003).

[2] M. Fox, "Optical properties of Solids", 1st edition , Oxford University Press, UK (2001).

[3] P. Markos and C. Soukoulis, "Wave Propagation From Electrons to Photonic Crystals and Left Handed Materials", 1st Edition, Prinston University Press, New Jersy (2008).

[4] F. Pillon, H. Gilles, S. Girard and M.Laroche, "Goos–Hänchen and Imbert–Fedorov shifts for leaky guided modes", J. Opt. Soc. Am. B, Vol. 22, No. 6, pp. 1290-1299 (2005).

[5] J. Hecht," City of lights: The story of Fiber Optics", 1st edition, Oxford University Press, UK (2004).

[6] F. Smith, T. King and D. Wilkins, "Optics and Photonics: An Introduction", 2nd edition, John Wiley & Sons ltd., New York USA (2007).

[7] J. Admams, "Introduction to Optical Waveguide", John Wiley & Sons Ltd., New York USA (1981).

[8] H. Mukundan, A. Anderson , W. Grace, K. Grace, N. Hartman, J. Martinez and B. Swanson, "Waveguide-Based Biosensors for Pathogen Detection", *Sensors*, Vol. *9*, No. 7, pp. 5783-5809 (2009).

[9] Y. Ren, Waveguide properties of thin Film Polymers, PhD Thesis, University of Durham (UK), 1999.

[10] N. Skiveseen, Metal-Clad Waveguide Sensors, PhD Thesis, University of Copenhagen (Denmark), 2005.

[11] N. Cennamo, Integrated Optical Planar Waveguides for Biosensors, PhD Thesis, Seconda Universita Delgi Studi di Napoli (Italy), 2005.

[12] A. Verma, Y. Prajapati, S. Ayub, J.P. Saini and V. Singh, "Analytical analysis of sensitivity of optical waveguide sensor", International Journal of Engineering, Science and Technology, Vol. 3, No. 3, pp. 36-40 (2011).

[13] G.C. Righini, A. Mignani, I. Cacciari and M. Brenci, "An Introduction to Optoelectronic Sensors", World Scientific Publishing Co. Pte. Ltd. (Singapore), 2009.

[14] M. Nirschl , F. Reuter, J. Vörös, " Review of Transducer Principles for Label-Free Biomolecular Interaction Analysis", Biosensors, Vol. 1, pp.70-92 (2011).

[15] X. Fan, I. M. White, S. Shopova, H. Zhu, J. Suter, Y. Sun, "Sensitive optical biosensors for unlabeled targets: A review", Analytica Chimica Acta, Vol. 620, pp. 8-26 (2008).

[16] H. Hunta, A. Armani, ” Label-free biological and chemical sensors", Nanoscale, Vol. 2, pp. 1544–1559 (2010).

[17] M. Cooper, "Label-Free Biosensors: Techniques and Applications", Cambridge University Press, UK (2009).

[18] O. Parriaux and P. Dieraur, "Normalized Expressions for the Optical Sensitivity of Evanescent Wave Sensors", Opt. Lett., Vol. 19, No. 7, pp. 508-510 (1994).

[19] Parriaux O. and Velduis G.J., "Normalized analysis for the sensitivity optimization of integrated optics evanescent wave sensors", J. of light Tech., Vol. 16,No. 4,p.p. : 573 – 582 (1998).

[20] T. El-Agez, S. Taya, "Theoretical Spectroscopic Scan of the Sensitivity of Asymmetric Slab Waveguide Sensors", Optica Applicata, Vol. 41, No. 1 (2011).

[21] S. A. Taya, T. M. El-Agez, Optical sensors based on Fabry–Perot resonator and fringes of equal thickness structure, Optik-International J. for Light and Electron Optics, Vol. 123, No. 5, pp. 418-422 (2012).

[22] N. Skivesen, R. Horvath, H.C. Pedersen, "Optimization of metal-clad waveguide sensors", Sensors and Actuators B 106, pp. 668–676 (2005).

[23] S. Taya, M. Shabat, H. Khalil, "Nonlinear Planar Asymmetrical Optical Waveguides for Sensing Applications", Optik, Vol. 121, pp. 860-865 (2010).

[24] S. Taya, M. Shabat, H. Khalil, D. Jäger, "Theoretical Analysis of TM Nonlinear Asymmetrical Waveguide Optical sensors", Sens. Actuat. A, Vol. 147, pp. 137-141 (2008).

[25] M. Shabat, H. Khalil, S. Taya, M. Abadla, "Analysis of the Sensitivity of Self-focused Nonlinear Optical Evanescent Waveguide Sensors", Int. J. Optomechatronics, Vol. 1, No. 1, pp. 284-296 (2007).

[26] H. Khalil, M. Shabat, S. Taya, M. Abadla, "Nonlinear Optical Waveguide Structure for Sensor Application: TM case", Int. J. Modern Phys. B, Vol.21, No. 30, pp. 5075-5089 (2007).

[27] R. Horvath, L. Lindvold, N. Larsen, "Reverse-symmetry Waveguides: Theory and Fabrication", App. Phys. B, Vol. 74, No. 4 , pp. 383-393 (2002).

[28] R. Horvath , H. Pederson , N. Larsen , "Demonstration of Reverse Symmetry Waveguide Sensing in Aqueous Solutions", App. Phys. Lett., Vol. 81, pp. 2166–2168 (2002).

[29] S. Taya , T. El-Agez , "Reverse Symmetry Optical Waveguide Sensor using Plasma Substrate", J. Opt., Vol.13, pp. 075701 (2011).

[30] S. Taya, M. Shabat, and H. Khalil, "Enhancement of Sensitivity in optical sensors using left-handed materials", Optik, Vol. 120, pp. 504-508 (2009).

[31] M. Abadla, S. Taya, and M. Shabat "Four-layer Slab Waveguide Sensors Supported with Left-Handed Materials", Sensor letters. Vol. 9, No. 5, 1823-1829, (2011).

[32] S. Taya, T. El-Agez, H. Kullab, M. Abadla, and M. Shabat, "Theoretical Study of Slab Waveguide Optical Sensor with Left-Handed Material as a Core Layer", Optica Applicata, Vol. 42, No. 2, p.p. 193-205 (2012).

[33] S. Taya, M. Abadla, M. Shabat, and E. El-Farram, "Evanescent Wave Sensors with a Left-Handed Material as a Substrate", Chinese J. of Physics, Vol. 50, No. 3, p.p. 478-499 (2012).

[34] H. Kullab, S. Taya, and T. El-Agez, "Metal-Clad Waveguide Sensor using a Left-Handed Material as a Core Layer", Journal of the Optical Society of America B, J. Opt. Soc. Am. B, Vol. 29, p.p. 959-964 (2012).

[35] T. El-Agez, S. Taya, M. Shabat, and H. Kullab, "Planar Waveguide with Left-Handed Material Guiding Film for Refractometry Applications", Turkish Journal of Physics, Vol. 37, p.p. 250-258 (2013).

[36] S. Khorasani and B. Rashidian, "Guided Light Propagation in Dielectric Slab Waveguide with Conducting Interfaces", Journal of Optics, Vol. 3, p.p. 380-386 (2001).

[37] K. Tiefenthaler and W. Lukosz, "Sensitivity of Grating Couplers as Integrated-Optical Chemical Sensors ", Optical Society of America, Vol. B, p.p. 209-220 (1989).